CHALMERS | UNIVERSITY OF GOTHENBURG

PREPRINT 2011:18

Domain Decomposition Finite Element/Finite Difference Approach for the Maxwell's System in Time Domain

LARISA BEILINA

Department of Mathematical Sciences
Division of Mathematics
CHALMERS UNIVERSITY OF TECHNOLOGY
UNIVERSITY OF GOTHENBURG
Gothenburg Sweden 2011

Preprint 2011:18

Domain Decomposition Finite Element/Finite Difference Approach for the Maxwell's System in Time Domain

Larisa Beilina

Department of Mathematical Sciences
Division of Mathematics
Chalmers University of Technology and University of Gothenburg
SE-412 96 Gothenburg, Sweden
Gothenburg, June 2011

Preprint 2011:18
ISSN 1652-9715

Matematiska vetenskaper
Göteborg 2011

DOMAIN DECOMPOSITION FINITE ELEMENT/FINITE DIFFERENCE APPROACH FOR THE MAXWELL'S SYSTEM IN TIME DOMAIN

LARISA BEILINA *

Abstract.
We present a new efficient fully explicit domain decomposition finite element/finite difference method for the numerical solution of Maxwell equations in the time domain. We also derive rigorously energy estimates for the second order vector wave equation with gauge condition for the electric field with non-constant electric permittivity function inside the domain where finite elements are used. Numerical experiments illustrate efficiency of the new scheme when it is applied to the solution of coefficient inverse problems.

1. Introduction. The goal of this paper is to present the new efficient domain decomposition FEM/FDM method which can be applied to the solution of the coefficient inverse problems (CIPs), for example, to reconstruct dielectric permittivity function $\varepsilon(x)$ of the medium under investigation with the condition that the electric permeability $\mu(x) = 1$ in the whole domain. Applications of the proposed domain decomposition FEM/FDM method for solutions of CIPs are broad - from the airport security to the imaging of land mines. In all such applications we reconstruct dielectric constant of explosives, and they are 3-5 times higher than ones of regular materials, see $http://www.clippercontrols.com$.

In many algorithms for the solution of electromagnetic CIPs we need accurately generate backscattered data at the boundary of the computational domain in order to reconstruct coefficient $\varepsilon(x)$ inside the medium. In this case the forward problems for PDEs are considered in the entire space $\mathbb{R}^3$, see for example [4, 5, 6, 16]. It is efficient to approximate the solution of these Cauchy problems via the solution of a boundary value problem in a bounded domain with $\varepsilon(x) = \mu(x) = 1$ in a neighborhood of the boundary of the computational domain, and with $\varepsilon(x) \neq const., \varepsilon(x) \geq 0$ in the rest of the domain. In this case the time-dependent Maxwell equations reduces to the system of independent wave equations in the neighborhood of the computational domain, and usage of the hybrid technique is preferable for the efficient solution of CIPs with coefficients which have properties described above.

Analytical part of this work presents proof of the energy estimate for the second order time-dependent Maxwell's system. We adopt the technique of [17] where the energy estimates was derived for a single hyperbolic equation. The main new element in our analysis is that we proof energy estimate for the time dependent Maxwell equation for the electric field with the Coulomb-type gauge condition in the presence of the first order absorbing boundary conditions [10].

The main idea of the proposed domain decomposition FEM/FDM method is following: we decompose the computational domain Ω into two subregions such that $\Omega = \Omega_{FEM} \cup \Omega_{FDM}$, where in Ω_{FEM} are used finite elements, and in Ω_{FDM} are used finite differences. We also note that in our algorithm Ω_{FEM} lies strictly inside Ω_{FDM} and thus corner singularities of the computational solution for the Maxwell's system in Ω_{FEM} are excluded. We assume that $\mu(x) = 1$ in the whole domain Ω. Next, in Ω_{FDM} we assume that $\varepsilon(x) = 1$ and we solve the usual system of wave equations with the first order absorbing boundary conditions [10] at the exterior boundary of the Ω_{FDM}. In Ω_{FEM}, however, the coefficient $\varepsilon \geq 0$, and we use the finite element method to solve Maxwell's system there. We also assume that both domains, Ω_{FEM} and Ω_{FDM}, overlaps in two layers of structured nodes, and in these nodes $\varepsilon(x) = 1$ as well. However, in Ω_{FEM} the mesh can be purely unstructured, and thus, adaptive algorithms can be applied there.

Efficiency of the proposed method is evident. It is well known, that the Finite Difference scheme is simple, but can be applied only on the structured (Cartesian) grids. From other side, Finite Element Methods (FEMs) can handle complex boundaries and unstructured grids. They also provide rigorous a posteriori error estimates which are useful for local adaptivity and error control. However, FEMs are more expensive than the Finite Difference method, both in computer time and in memory requirement. The proposed domain decomposition scheme combines the advantages of the two methods.

* Department of Mathematical Sciences, Chalmers University of Technology and Gothenburg University, SE-42196 Gothenburg, Sweden, (larisa@chalmers.se)

The numerical implementation of the proposed domain decomposition method is following. We use the explicit finite difference method in Ω_{FDM} similar to one used in [2]. For the finite element discretization of Maxwell equations in Ω_{FEM}, however, we use the node-based curl-curl formulation with the divergence free condition which is similar to [3]. The proposed domain decomposition method of this paper is free from instabilities which can occur when the two methods are hybridized since our Maxwell's system overcame to the system of wave equations at the overlapping nodes between Ω_{FEM} and Ω_{FDM}.

It is known that edge elements are the most satisfactory from a theoretical point of view [18] since they automatically satisfy the divergence free condition. However, they are less attractive for time dependent computations, since the solution of a linear system is required at every time iteration. In addition, in the case of triangular or tetrahedral edge elements, the entries of the diagonal matrix resulting from mass-lumping are not necessarily strictly positive [9]; therefore, explicit time stepping cannot be used in general. In contrast, nodal elements naturally lead to a fully explicit scheme when mass-lumping is applied [9, 15]. However, numerical solutions of Maxwell equations using nodal finite elements may contain spurious solutions [19, 22], and various techniques are available to remove them [12, 13, 14, 21, 22]. We eliminate the spurious solutions by adding the divergence condition to the time dependent equation for the electric field, which removes spurious solutions when local mesh refinement is applied and material discontinuities are not too big [3]. Our numerical tests of section 7 show that in the case of CIPs similar to ones of [6, 16], these spurious solutions will not appear.

Now we explain the meaning of numerical tests performed in section 7.2, where we present numerical verification of the proposed domain decomposition method for the solution of the Maxwell's system in time domain with initialized plane wave which is similar to one used in tests of [6, 16]. The reason to do it is following. In [6, 16] we have presented the reconstruction of refractive indexes of abnormalities from experimental data. In these works for solution of the electromagnetic CIP was used the simplified mathematical model of the single wave equation instead of the full Maxwell's system. Despite of this discrepancy, in [6] was obtained excellent accuracy of the reconstruction of both locations and refractive indices of dielectrics. In addition, using the adaptivity technique the shape of the dielectric abnormalities was also reconstructed accurately. This can be explained by the fact that the data immersing procedure of [6, 16] smoothed out the data, and thus, enforced them to be good for the considered model of the wave equation.

Our conclusion from the numerical test of section 7.2 with a plane wave is that all meaningful reflections from the abnormalities inside the Ω_{FEM} are only from the one component of the electric field while the reflections from the other component are negligible. This test explains results of experiments performed in [6, 16] when physicists could measure only one component of the electric field. Because of that in [6, 16] we have approximated our model problem of Maxwells equations with the single wave equation. Tests of section 7 illustrate results of [16, 6] when in some experiments with the plane wave it is reasonable approximate the full Maxwell's system with the single wave equation. However, in our future work we plan apply the method developed in this paper for the solution of CIPs similar to ones in [6, 16], but for the full Maxwell's system, and compare results.

The outline of the work is as follows. In section 2 we briefly recall Maxwell equations and in section 3 we present the mathematical model which we consider in this work. In section 4 we derive the energy estimate. Then in section 5 we present the finite element method and in section 5.1 - the explicit scheme for the electric field. The finite difference scheme is summarized in section 5.2, and the first order absorbing boundary conditions for this sheme is presented in section 5.3. Next, we formulate the hybrid FEM/FDM method in section 6. Finally, in section 7 we present numerical examples which demonstrate the efficiency of our adaptive hybrid FEM/FDM solver.

2. Maxwell equations. Let $\Omega \subset \mathbb{R}^3$ be a bounded domain with a piecewise smooth boundary $\partial\Omega$, $T = const. > 0$. Let $L^2(\Omega)$ will be the space of square integrable functions in Ω. Let's define $\Omega_T := \Omega \times (0, T)$, $\partial\Omega_T := \partial\Omega \times (0, T)$.

We consider Maxwell equations in an inhomogeneous isotropic medium in a bounded domain Ω_T:

$$\begin{aligned} \frac{\partial D}{\partial t} - \nabla \times H &= -J, \text{ in } \Omega_T, \\ \frac{\partial B}{\partial t} + \nabla \times E &= 0, \text{ in } \Omega_T, \\ D &= \varepsilon E, \\ B &= \mu H, \\ E(x,0) &= E_0(x), \\ H(x,0) &= H_0(x). \end{aligned} \tag{2.1}$$

Here $E(x,t)$ and $H(x,t)$ are the electric and magnetic fields, whereas $D(x,t)$ and $B(x,t)$ are the electric and magnetic inductions, respectively. The dielectric permittivity, $\varepsilon(x) > 0$, and magnetic permeability, $\mu(x) > 0$, together with the current density, $J(x,t) \in \mathbb{R}^3$, are given and assumed piecewise smooth. Moreover, the electric and magnetic inductions satisfy the relations

$$\nabla \cdot D = \rho, \ \nabla \cdot B = 0 \qquad \text{in } \Omega_T, \tag{2.2}$$

where $\rho(x,t)$ is a given charge density.

Traditionally perfectly conducting boundary conditions for (2.1), (2.2) are the most popular ones

$$\begin{aligned} n \times E &= 0, \qquad \text{on } \partial\Omega_T \\ H \cdot n &= 0, \qquad \text{on } \partial\Omega_T. \end{aligned} \tag{2.3}$$

Here n denotes the outward normal on $\partial\Omega$.

However, our goal is to construct an efficient solver for the forward problem (2.1) in order to generate the data at $\partial\Omega$ to solve then Coefficient Inverse Problems (CIPs). As we have mentioned above, in the case of CIPs forward problems are usually Cauchy problems. Therefore, we need to approximate the solution of the Cauchy problem via the solution of a boundary value problem in a bounded domain. On the other hand, if $\varepsilon(x), \mu(x) = const. > 0$ in a neighborhood Ω' of $\partial\Omega$, as it is often the case in CIPs, then it is well known that for $(x,t) \in \Omega' \times (0,T)$ from (2.1) one obtains independent vector wave equations

$$\begin{aligned} \varepsilon\mu\partial_t^2 E - \Delta E &= -j \\ \varepsilon\mu\partial_t^2 H - \Delta H &= \frac{1}{\varepsilon}\nabla \times J, \end{aligned} \tag{2.4}$$

where $j = \frac{\partial J}{\partial t}$. When solving the CIPs in real-life applications such as in subsurface imaging or in detecting of explosives, it is efficient bound the domain of interest by artificial boundary and impose absorbing boundary conditions. First order absorbing boundary conditions [10] work quite well for the case of a single hyperbolic PDE [4, 5] in the case when the plane wave is initialized in orthogonal direction to the some part of the boundary $\partial\Omega$. Hence, by analogy, in this work we consider first order absorbing boundary conditions at $\partial\Omega_T$ for the Maxwell equations.

By eliminating B and D from (2.1) we obtain the two independent second order systems of partial differential equations

$$\varepsilon\frac{\partial^2 E}{\partial t^2} + \nabla \times (\mu^{-1}\nabla \times E) = -j, \tag{2.5}$$

$$\mu\frac{\partial^2 H}{\partial t^2} + \nabla \times (\varepsilon^{-1}\nabla \times H) = \nabla \times (\varepsilon^{-1} J), \tag{2.6}$$

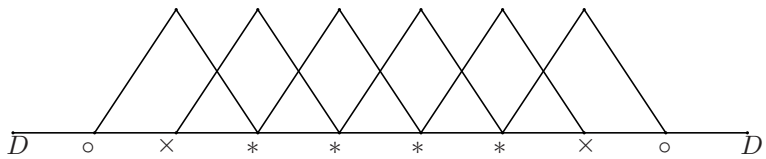

Fig. 3.1: Domain decomposition between Ω_{FEM} and Ω_{FDM} in one dimension. The interior nodes of the unstructured finite element grid are denoted by stars, while circles and crosses denote nodes, which are shared between meshes in Ω_{FEM} and Ω_{FDM}. The circles are interior nodes ω_0 of the grid in Ω_{FDM}, while the crosses are interior nodes ω_x of the grid in Ω_{FEM}. At each time iteration, solution obtained in Ω_{FDM} at ω_0 is copied to the corresponding nodes in Ω_{FEM}, while simultaneously the solution obtained in Ω_{FEM} at ω_x is copied to the corresponding nodes in Ω_{FDM}.

The initial conditions are

$$E(x,0) = E_0(x), \tag{2.7}$$

$$H(x,0) = H_0(x), \tag{2.8}$$

$$\frac{\partial E}{\partial t}(x,0) = (\nabla \times H_0(x) - J(x,0))/\varepsilon(x), \tag{2.9}$$

$$\frac{\partial H}{\partial t}(x,0) = -\nabla \times E_0/\mu(x). \tag{2.10}$$

3. Mathematical models. We are interesting in solution of the equation (2.5) for the electric field with first order absorbing boundary conditions and appropriate initial conditions. For the above described setting of the problem it is convenient to use domain decomposition finite element/finite difference method. In doing so we decompose Ω into two subregions, Ω_{FEM} and Ω_{FDM} such that $\Omega = \Omega_{FEM} \cup \Omega_{FDM}$, see Figure 3.1. Ω_{FEM} corresponds to the domain, where finite elements are used, and lies strictly inside Ω_{FDM}. In Ω_{FDM} we will use finite difference method with first order absorbing boundary conditions.

We also assume that we are working in nonconducting medium, what means that the charge density $\rho = 0$. Our next assumption is that the magnetic permeability $\mu(x) = 1 \quad \forall x \in \Omega$, and we let the electric permittivity $\varepsilon(x)$ to be such that

$$\begin{aligned} &\varepsilon(x) \geq 1, \text{ for } x \in \Omega_{FEM}, \ \varepsilon(x) \in C^2(\bar{\Omega}), \\ &\varepsilon(x) = 1, \text{ for } x \in \Omega_{FDM}. \end{aligned} \tag{3.1}$$

Let us formulate the model problem for the electric field E with the first order absorbing boundary conditions [10] at the boundary $\partial\Omega$

$$\varepsilon \frac{\partial^2 E}{\partial t^2} + \nabla \times (\nabla \times E) = -j, \text{ in } \Omega_T, \tag{3.2}$$

$$\nabla \cdot (\varepsilon E) = 0, \text{ in } \Omega_T, \tag{3.3}$$

$$E(x,0) = f_0(x), \quad E_t(x,0) = f_1(x) \text{ in } \Omega, \tag{3.4}$$

$$\partial_n E(x,t) = -\partial_t E(x,t) \text{ on } \partial\Omega_T. \tag{3.5}$$

Here we assume that

$$j \in L_2(\Omega_T), f_0 \in H^1(\Omega), f_1 \in L_2(\Omega). \tag{3.6}$$

As we have mentioned above, we will use domain decomposition finite element/finite difference method for the numerical solution of (3.2)-(3.5). This means that for solution (3.2)-(3.5) in Ω_{FDM} we shall use the finite difference method on a structured mesh with constant coefficients $\varepsilon = \mu = 1$. As we have pointed out in section 2 in this case the problem (3.2)-(3.5) transforms to the system of vector wave equations (2.4).

In Ω_{FEM}, however, we shall use finite elements on a sequence of non-degenerate unstructured meshes $K_h = \{K\}$, with elements K consisting of triangles in $\mathbb{R}^2$ and tetrahedra in $\mathbb{R}^3$ [7]. Efficiency of the resulting domain decomposition FEM/FDM scheme in Ω is obtained by using mass lumping in both space and time in Ω_{FEM}, which makes the scheme fully explicit [11]. In Ω_{FEM} we associate with K_h a (continuous) mesh function $h = h(x)$, which represents the diameter of the element K that contains x. For the time discretization we let $J_\tau = \{J\}$ be a partition of the time interval $I = [0, T]$, where $0 = t_0 < t_1 < ... < t_N = T$ is a sequence of discrete time steps with associated time intervals $J = (t_{k-1}, t_k]$ of constant length $\tau = t_k - t_{k-1}$.

Below for any vector function $u \in \mathbb{R}^3$ our notations $u \in L^2(\Omega)$ or $u \in H^k(\Omega), k = 1, 2$ mean that every component of the vector function u belongs to this space.

Keeping above remark in mind, it is well known that when using standard, piecewise continuous $H^1(\Omega)$-conforming FE for the numerical solution of Maxwell equations, we have following difficulties. First, in general the solution of (2.5) lies in the space $H_0(\text{curl}, \Omega) \cap H(\text{div}, \Omega)$ with

$$H_0(\text{curl}, \Omega) := \{u \in L^2(\Omega) : \nabla \times u \in L^2(\Omega), \quad u \times n = 0\}, \tag{3.7}$$

and

$$H(\text{div}, \Omega) := \{u \in L^2(\Omega) : \nabla \cdot u \in L^2(\Omega)\}, \tag{3.8}$$

here n is the unit outward normal to $\partial\Omega$. The space $H_0(\text{curl}, \Omega) \cap H(\text{div}, \Omega)$ is strictly larger than $[H^1(\Omega)]^3$ when Ω has re-entrant corners ([18], p.191). However, this restriction is of no concern in our method, because we will use finite elements only in Ω_{FEM}, which lies strictly inside Ω; hence, in our case corner singularities are excluded. Second, because the bilinear form $a(u, v) = (\nabla \times u, \nabla \times v)$ is not coercive without some (at least weak) restriction to divergence-free functions, direct application of the finite element method to the numerical solution of Maxwell equations using $H^1(\Omega)$-conforming nodal finite elements can result in spurious solutions (the finite element solution does not satisfy the divergence condition (3.3)). To remove these spurious solutions from the finite element solution, we shall add a Coulomb-type gauge condition to enforce the divergence condition [1, 21, 22].

Thus, we modify equations (3.2) - (3.5) with $s \geq 1$ as

$$\varepsilon \frac{\partial^2 E}{\partial t^2} + \nabla \times (\nabla \times E) - s\nabla(\nabla \cdot (\varepsilon E)) = -j, \text{ in } \Omega_T, \tag{3.9}$$

$$E(x, 0) = f_0(x), \quad E_t(x, 0) = f_1(x) \text{ in } \Omega, \tag{3.10}$$

$$\partial_n E(x, t) = -\partial_t E(x, t), \quad \nabla \cdot E = 0 \text{ on } \partial\Omega_T. \tag{3.11}$$

$$\nabla \cdot E = 0 \text{ in } \Omega' \subset \Omega_{FDM}, \quad \varepsilon(x) = 1 \text{ in } \Omega_{FDM}, \tag{3.12}$$

where the subdomain Ω' is a small neighborhood of the outer boundary $\partial\Omega$. We note that as soon as the term $-s\nabla(\nabla \cdot (\varepsilon E))$ is incorporated in equation (3.9), equation $\nabla \cdot E = 0$ in $\Omega' \subset \Omega_{FDM}$ in (3.12) is an over-determination. On the other hand, this over-determination takes place only in a small neighborhood of the boundary $\partial\Omega$ rather than in the entire domain Ω. Likewise, we do not use (3.12) in our numerical experiments.

Since the modified bilinear form $a(u, v) = (\nabla \times u, \nabla \times v) + s(\nabla \cdot u, \nabla \cdot v)$ is now coercive on $H^1(\Omega)$ [23], the problem (3.9)-(3.11) is now well-posed. The addition of the term $s(\nabla \cdot u, \nabla \cdot v)$ does not change either solution of (3.9)-(3.11), but only provides a stabilization of the variational formulation - see also ([18], p.191).

Using the transformation (2.2) problem (3.9)-(3.11) can be rewritten as

$$\varepsilon \frac{\partial^2 E}{\partial t^2} + \nabla(\nabla \cdot E) - \nabla \cdot (\nabla E) - s\nabla(\nabla \cdot (\varepsilon E)) = -j, \text{ in } \Omega_T, \tag{3.13}$$

$$E(x, 0) = f_0(x), \quad E_t(x, 0) = f_1(x) \text{ in } \Omega, \tag{3.14}$$

$$\partial_n E(x, t) = -\partial_t E(x, t), \quad \nabla \cdot E = 0 \text{ on } \partial\Omega_T. \tag{3.15}$$

$$\nabla \cdot E = 0 \text{ in } \Omega' \subset \Omega_{FDM}, \quad \varepsilon(x) = 1 \text{ in } \Omega_{FDM}. \tag{3.16}$$

4. Energy estimate for the problem (3.13)-(3.16). In this section we proof the uniqueness theorem, or energy estimate, for the vector $E \in H^2(\Omega_T)$ of the equation (3.13)-(3.16), using the technique of [17] where the energy error estimates was derived for a single hyperbolic equation.

Theorem

Assume that condition (3.1) on the coefficient $\varepsilon(x)$ hold. Let $\Omega \subset \mathbb{R}^3$ be a bounded domain with the piecewise smooth boundary $\partial\Omega$. For any $t \in (0,T)$ let $\Omega_t = \Omega \times (0,t)$. Suppose that there exists a solution $E \in H^2(\Omega_T)$ of the equation (3.13)-(3.16). Then the vector E is unique and there exists a constant $B = B(||\varepsilon||_\Omega, t, s)$ depending only on the $||\varepsilon||_\Omega$, t and s such that the following energy estimate is true for all s such that $s\varepsilon \geq 1$ in (3.13)-(3.16)

$$\begin{aligned} &\left\|\sqrt{\varepsilon}\partial_t E(x,t)\right\|^2_{L_2(\Omega)} + \|\nabla E(x,t)\|^2_{L_2(\Omega)} + \left\|\sqrt{s\varepsilon-1}\nabla\cdot E(x,t)\right\|^2_{L_2(\Omega)} \\ &\leq B\left[\|j\|^2_{L_2(\Omega_t)} + \left\|\sqrt{\varepsilon}f_1\right\|^2_{L_2(\Omega)} + \|\nabla f_0\|^2_{L_2(\Omega)} + \|f_0\|^2_{L_2(\Omega)} + \left\|\sqrt{s\varepsilon-1}\,\nabla\cdot f_0\right\|^2_{L_2(\Omega)}\right]. \end{aligned} \tag{4.1}$$

Proof.

First we multiply (3.13) by $2\partial_t E$ and integrate over $\Omega \times (0,t)$ to get

$$\begin{aligned} &\int_0^t\int_\Omega 2\,\varepsilon\partial_{tt}E\;\partial_t E\;dxd\tau + \int_0^t\int_\Omega 2\nabla(\nabla\cdot E)\;\partial_t E\;dxd\tau - \int_0^t\int_\Omega 2\nabla\cdot(\nabla E)\;\partial_t E\;dxd\tau \\ &- s\int_0^t\int_\Omega 2\nabla(\nabla\cdot(\varepsilon E))\;\partial_t E\;dxd\tau = -2\int_0^t\int_\Omega j\;\partial_t E\;dxd\tau. \end{aligned} \tag{4.2}$$

Integrating in time the first term of (4.2) we get

$$\int_0^t\int_\Omega \partial_t(\varepsilon\partial_t E^2)dxd\tau = \int_\Omega \left(\varepsilon\partial_t E^2\right)(x,t)\,dx - \int_\Omega \varepsilon f_1^2(x,t)\,dx. \tag{4.3}$$

Integrating by parts in space the second term of (4.2), which corresponds to the divergence, we have

$$\begin{aligned} &2\int_0^t\int_\Omega \nabla(\nabla\cdot E)\,\partial_t E dxd\tau \\ &= 2\int_0^t\int_{\partial\Omega} \partial_t E\;n\cdot(\nabla\cdot E)dSd\tau - 2\int_0^t\int_\Omega (\nabla\cdot E)(\nabla\cdot\partial_t E)\,dxd\tau \\ &= 2\int_0^t\int_{\partial\Omega} \partial_t E\;n\cdot(\nabla\cdot E)dSd\tau - \int_0^t\int_\Omega \partial_t(\nabla\cdot E)^2\,dxd\tau. \end{aligned} \tag{4.4}$$

The term $2\int_0^t\int_{\partial\Omega} \partial_t E n\cdot(\nabla\cdot E)dSd\tau = 0$ since by (3.16) $\nabla\cdot E = 0$ in a small neighbourhood of the $\partial\Omega$.

Next, integrating the last term of (4.4) in time and using (3.14) we have

$$\begin{aligned} &-\int_0^t\int_\Omega \partial_t(\nabla\cdot E)^2\,dxd\tau = -\int_\Omega (\nabla\cdot E)^2(x,t)\,dx + \int_\Omega (\nabla\cdot E)^2(x,0)\,dx \\ &= -\int_\Omega (\nabla\cdot E)^2(x,t)\,dx + \int_\Omega (\nabla\cdot f_0)^2(x)\,dx. \end{aligned} \tag{4.5}$$

Integrating by parts in space the third term of (4.2) corresponding to the gradient, and using (3.14) we get

$$
\begin{aligned}
&2\int_0^t\int_\Omega \nabla\cdot(\nabla E)\,\partial_t E dx d\tau \\
&= 2\int_0^t\int_{\partial\Omega} (\partial_t E)\,\partial_n E dS d\tau - 2\int_0^t\int_\Omega (\nabla E)\,(\nabla\partial_t E)\,dx d\tau \\
&= -2\int_0^t\int_{\partial\Omega} (\partial_t E)^2\ dS d\tau - \int_0^t\int_\Omega \partial_t|\nabla E|^2 dx d\tau,
\end{aligned}
\tag{4.6}
$$

Integrating last term of (4.6) in time and using (3.14) we obtain

$$
\begin{aligned}
&-\int_0^t\int_\Omega \partial_t|\nabla E|^2 dx d\tau = -\int_\Omega |\nabla E|^2\,(x,t)\,dx + \int_\Omega |\nabla E|^2\,(x,0)\,dx \\
&= -\int_\Omega |\nabla E|^2\,(x,t)\,dx + \int_\Omega |\nabla f_0|^2\,(x)\,dx.
\end{aligned}
\tag{4.7}
$$

Integrating in space the augmented term of (4.2) we have

$$
\begin{aligned}
&2s\int_0^t\int_\Omega \nabla\,(\nabla\cdot(\varepsilon E))\,\partial_t E dx d\tau \\
&= 2s\int_0^t\int_{\partial\Omega} \partial_t E\ n\cdot(\nabla\cdot(\varepsilon E)) dS d\tau - 2s\int_0^t\int_\Omega (\nabla\cdot(\varepsilon E))\,(\nabla\cdot\partial_t E)\,dx d\tau \\
&= 2s\int_0^t\int_{\partial\Omega} \partial_t E\ n\cdot(\nabla\cdot(\varepsilon E)) dS d\tau - 2s\int_0^t\int_\Omega (\nabla\varepsilon\cdot E)\nabla\cdot(\partial_t E) dx d\tau - s\int_0^t\int_\Omega \varepsilon\partial_t(\nabla\cdot E)^2\,dx d\tau.
\end{aligned}
\tag{4.8}
$$

The term $2s\int_0^t\int_{\partial\Omega} \partial_t E\ n\cdot(\nabla\cdot(\varepsilon E)) dS d\tau = 0$ since $\varepsilon = 1$ on the boundary $\partial\Omega$, and by (3.16) $\nabla\cdot E = 0$ on a small neighbourhood of the $\partial\Omega$.

Next, integrating in space one more time the term $2s\int_0^t\int_\Omega (\nabla\varepsilon\cdot E)\nabla\cdot(\partial_t E) dx d\tau$ in (4.8) we have

$$
\begin{aligned}
&-2s\int_0^t\int_\Omega (\nabla\varepsilon\cdot E)\nabla\cdot(\partial_t E) dx d\tau \\
&= -2s\int_0^t\int_{\partial\Omega} (\nabla\varepsilon\cdot E) n\cdot(\partial_t E) dx d\tau + 2s\int_0^t\int_\Omega \nabla(\nabla\varepsilon\cdot E)(\partial_t E) dx d\tau = 2s\int_0^t\int_\Omega \nabla(\nabla\varepsilon\cdot E)\partial_t E\ dx d\tau.
\end{aligned}
\tag{4.9}
$$

Here, the integral $-2s\int_0^t\int_{\partial\Omega} (\nabla\varepsilon\cdot E) n\cdot(\partial_t E) dx d\tau = 0$ since $\varepsilon = 1$ in a small neighbourhood of the $\partial\Omega$ and hence $\nabla\varepsilon = 0$ in this neighbourhood.

Next, collecting estimates (4.3), (4.4) (4.5), (4.6), (4.7), (4.8), (4.20), using the fact that $2\int\limits_0^t\int\limits_{\partial\Omega}\left(\partial_t E\right)^2\, dSd\tau \geq 0$ and substituting them in (4.2) we have

$$\begin{aligned}
&\int\limits_\Omega \left(\varepsilon\partial_t E^2\right)(x,t)\,dx - \int\limits_\Omega \left(\nabla\cdot E\right)^2(x,t)\,dx + \int\limits_\Omega |\nabla E|^2(x,t)\,dx \\
&+ s\int\limits_0^t\int\limits_\Omega \varepsilon\partial_t(\nabla\cdot E)^2\,dxd\tau \leq 2\int\limits_0^t\int\limits_\Omega |j|\,|\partial_t E|\,dxd\tau + \int\limits_\Omega \varepsilon f_1^2(x,t)\,dx - \int\limits_\Omega (\nabla\cdot f_0)^2(x)\,dx \\
&+ \int\limits_\Omega |\nabla f_0|^2(x)\,dx + 2s\int\limits_0^t\int\limits_\Omega |\nabla(\nabla\varepsilon\cdot E)||\partial_t E|\,dxd\tau.
\end{aligned} \tag{4.10}$$

Let $A = A(||\varepsilon||_{C^2(\Omega)}, s) > 0$ denotes the constant depending only on the $||\varepsilon||_\Omega$ and t, s. Now we can write estimate

$$|\nabla(\nabla\varepsilon\cdot E)| \leq A(|E| + |\nabla E|).$$

Using the estimate above and the inequality $2ab \leq a^2 + b^2$ we estimate the last term in the equation (4.10) as

$$2s\int\limits_0^t\int\limits_\Omega |\nabla(\nabla\varepsilon\cdot E)||\partial_t E|\,dxd\tau \leq 2sA\int\limits_0^t\int\limits_\Omega |\partial_t E|\cdot(|E| + |\nabla E|)\,dxd\tau. \tag{4.11}$$

With another constant A we have

$$2s\int\limits_0^t\int\limits_\Omega |\nabla(\nabla\varepsilon\cdot E)||\partial_t E|\,dxd\tau \leq A\int\limits_0^t\int\limits_\Omega |\partial_t E|^2\,dxd\tau + A\int\limits_0^t\int\limits_\Omega (|E| + |\nabla E|)^2\,dxd\tau. \tag{4.12}$$

The second integral in the right hand side of (4.11) can be estimated as

$$A\int\limits_0^t\int\limits_\Omega (|E| + |\nabla E|)^2\,dxd\tau \leq 2A\int\limits_0^t\int\limits_\Omega |E|^2\,dxd\tau + 2A\int\limits_0^t\int\limits_\Omega |\nabla E|^2\,dxd\tau. \tag{4.13}$$

Let us estimate the term $\int\limits_0^t\int\limits_\Omega |E|^2\,dxd\tau$ in (4.13). First we make the transformation

$$E(x,t) = E(x,0) + \int\limits_0^t \partial_t E\,dxd\tau. \tag{4.14}$$

Taking square of (4.14), integrating result in space and using the estimate $(a+b)^2 \leq 2a^2 + 2b^2$ we get

$$\int\limits_\Omega |E|^2\,dx \leq 2\int\limits_\Omega |E|^2(x,0)\,dx + 2\int\limits_\Omega \Big(\int\limits_0^t |\partial_t E|\,d\tau\Big)^2 dx \leq 2\int\limits_\Omega |E|^2(x,0)\,dx + 2t\int\limits_0^t\int\limits_\Omega |\partial_t E|^2\,d\tau dx. \tag{4.15}$$

Using the initial condition (3.14) we have

$$\int\limits_\Omega |E|^2\,dx \leq 2||f_0||^2_{L_2(\Omega)} + 2t\int\limits_0^t\int\limits_\Omega |\partial_t E|^2\,d\tau dx. \tag{4.16}$$

Integrating the above equation in the time $(0,t)$ we get

$$\int_0^t \int_\Omega |E|^2 \, dxd\tau \leq 2t||f_0||^2_{L_2(\Omega)} + 2t^2 \int_0^t \int_\Omega |\partial_t E|^2 \, d\tau dx. \tag{4.17}$$

Substituting the above expression in (4.11) and using (4.13) with the constant $B = B(||\varepsilon||_{C^2(\Omega)}, t, s) > 0$ we get

$$\begin{aligned} A \int_0^t \int_\Omega (|\partial_t E|^2 + |\nabla E|^2) \, dxd\tau &\leq 2A(2t||f_0||^2_{L_2(\Omega)} + 2t^2 \int_0^t \int_\Omega |\partial_t E|^2 \, d\tau dx) + 2A \int_0^t \int_\Omega |\nabla E|^2 dxd\tau \\ &\leq B \int_0^t \int_\Omega (|\partial_t E|^2 + |\nabla E|^2) \, dxd\tau + B \int_\Omega f_0^2 dx, \end{aligned} \tag{4.18}$$

and thus we get the following estimate for the augmented term in (4.10)

$$2s \int_0^t \int_\Omega |\nabla(\nabla\varepsilon \cdot E)||\partial_t E| \, dxd\tau \leq A \int_0^t \int_\Omega (|\partial_t E|^2 + |\nabla E|^2) \, dxd\tau + A \int_\Omega f_0^2 dx. \tag{4.19}$$

Now we estimate the rest of terms in (4.10). Integrating the fourth term of (4.10) in time we get

$$\begin{aligned} s \int_0^t \int_\Omega \varepsilon \partial_t \left(\nabla \cdot E\right)^2 dxd\tau &= s \int_\Omega \varepsilon \left(\nabla \cdot E\right)^2 (x,t) \, dx - s \int_\Omega \varepsilon \left(\nabla \cdot E\right)^2 (x,0) \, dx \\ &= s \int_\Omega \varepsilon \left(\nabla \cdot E\right)^2 (x,t) \, dx - s \int_\Omega \varepsilon \left(\nabla \cdot f_0\right)^2 (x) \, dx. \end{aligned} \tag{4.20}$$

Finally, to estimate the first term in the right hand side of (4.10) we use the arithmetic-geometric mean inequality $2ab \leq a^2 + b^2$ to obtain

$$2 \int_0^t \int_\Omega |j| \cdot |\partial_t E| \, dxd\tau \leq \int_0^t \int_\Omega |j|^2 dxd\tau + \int_0^t \int_\Omega |\partial_t E|^2 dxd\tau. \tag{4.21}$$

Noting that by (3.1) $\forall \varepsilon : s\varepsilon \geq 1$ we have

$$B \int_0^t \int_\Omega (|\partial_t E|^2 + |\nabla E|^2) \, dxd\tau \leq B \int_0^t \int_\Omega (\varepsilon |\partial_t E|^2 + (s\varepsilon - 1)(\nabla \cdot E)^2 + |\nabla E|^2) \, dxd\tau,$$

and substituting (4.19), (4.20), (4.21) into (4.10), we have the following estimate $\forall s\varepsilon - 1 \geq 0$

$$\begin{aligned} &\int_\Omega (\varepsilon \partial_t E^2 + |\nabla E|^2 + (s\varepsilon - 1)(\nabla \cdot E)^2) \, (x,t) \, dx \\ &\qquad \leq \int_0^t \int_\Omega |j|^2 dxd\tau + B \int_0^t \int_\Omega (\varepsilon |\partial_t E|^2 + (s\varepsilon - 1)(\nabla \cdot E)^2 + |\nabla E|^2) \, dxd\tau \\ &\qquad + \int_\Omega \left(\varepsilon f_1^2 + |\nabla f_0|^2 + (s\varepsilon - 1)(\nabla \cdot f_0)^2 + B f_0^2\right) (x,t) \, dx. \end{aligned} \tag{4.22}$$

Let us denote

$$F(t) := \int\limits_{\Omega} \left(\varepsilon \partial_t E^2 + |\nabla E|^2 + (s\varepsilon - 1)(\nabla \cdot E)^2)\right)(x,t)\, dx. \tag{4.23}$$

Then we can rewrite estimate (4.22) in the form

$$F(t) \le B \int_0^t F(\tau) d\tau + g(t), \tag{4.24}$$

where $g(t) := \int\limits_0^t \int\limits_{\Omega} |j|^2 dx d\tau + \int\limits_{\Omega} \left(\varepsilon f_1^2 + |\nabla f_0|^2 + (s\varepsilon - 1)(\nabla \cdot f_0)^2 + A f_0^2\right)(x,t)\, dx.$

Applying Gronwall's inequality to (4.24) with a different constant B we get desired estimate $\forall s\varepsilon \ge 1$

$$\begin{aligned} &\int\limits_{\Omega} \left(\varepsilon \partial_t E^2 + |\nabla E|^2 + (s\varepsilon - 1)(\nabla \cdot E)^2\right)(x,t)\, dx \\ &\qquad \le B\Big(\int\limits_0^t \int\limits_{\Omega} |j|^2 dx d\tau + \int\limits_{\Omega} \left(\varepsilon f_1^2 + |\nabla f_0|^2 + (s\varepsilon - 1)(\nabla \cdot f_0)^2 + f_0^2\right)(x,t)\, dx\Big). \end{aligned} \tag{4.25}$$

□

5. The finite element method . We will formulate the finite element method for the problem (3.9)-(3.11) with $f_0 = f_1 = 0$, which can be written as

$$\varepsilon \frac{\partial^2 E}{\partial t^2} + \nabla(\nabla \cdot E) - \nabla \cdot (\nabla E) - s\nabla(\nabla \cdot (\varepsilon E)) = -j, \text{ in } \Omega_T, \tag{5.1}$$

$$E(x,0) = 0, \quad E_t(x,0) = 0 \text{ in } \Omega, \tag{5.2}$$

$$\partial_n E(x,t) = -\partial_t E(x,t) \text{ on } \partial\Omega_T, \tag{5.3}$$

$$\nabla \cdot E = 0, \text{ on } \partial\Omega_T, \tag{5.4}$$

$$\nabla \cdot E = 0 \text{ in } \Omega' \subset \Omega_{FDM}, \varepsilon(x) = 1 \text{ in } \Omega_{FDM}. \tag{5.5}$$

First we introduce the finite element trial space W_h^E, defined by

$$W_h^E := \{w \in W^E : w|_{K\times J} \in [P_1(K)]^3 \times P_1(J), \forall K \in K_h, \forall J \in J_\tau\},$$

where $P_1(K)$ and $P_1(J)$ denote the set of linear functions on K and J, respectively, and

$$W^E := \{w \in [H^1(\Omega)]^3 \times I) : w(\cdot,0) = 0, \partial_n w|_{\partial\Omega} = -\partial_t w\}.$$

We also introduce the finite element test space W_h^φ defined by

$$W_h^\varphi := \{w \in W^\varphi : w|_{K\times J} \in [P_1(K)]^3 \times P_1(J), \forall K \in K_h, \forall J \in J_\tau\},$$

where

$$W^\varphi := \{w \in [H^1(\Omega)]^3 \times I) : w(\cdot,T) = 0, \partial_n w|_{\partial\Omega} = -\partial_t w\}.$$

Hence, the finite element spaces W_h^E and W_h^φ consist of continuous piecewise linear functions in space and time, which satisfy certain homogeneous initial and first order absorbing boundary conditions. We also define the following L_2 inner products and norms

$$((p,q)) = \int_\Omega \int_0^T pq\, dx\, dt, \quad \|p\|^2 = ((p,p)),$$

$$(\alpha,\beta)=\int_\Omega \alpha\beta\,dx,\quad |\alpha|^2=(\alpha,\alpha).$$

The finite element method for (3.13)- (3.16) reads: Find $E_h\in W_h^E$ such that $\forall\bar\varphi\in W_h^\varphi$,

$$\begin{aligned}&-((\varepsilon\frac{\partial E_h^k}{\partial t},\frac{\partial\bar\varphi}{\partial t}))-((\nabla\cdot E_h^k,\nabla\cdot\bar\varphi))+((\partial_t E_h^k,\bar\varphi))_{\partial\Omega}\\&+((\nabla E_h^k,\nabla\bar\varphi))+s((\nabla\cdot(\varepsilon E_h^k),\nabla\cdot\bar\varphi))+((j^k,\bar\varphi))=0.\end{aligned}\tag{5.6}$$

Here, the initial condition $\frac{\partial E}{\partial t}(x,0)=0$ is imposed weakly through the variational formulation.

5.1. The explicit scheme for the electric field. We expand $E(x,t)$ in terms of the standard continuous piecewise linear functions $\{\varphi_i\}_{i=1}^M$ in space and $\{\psi_k\}_{k=1}^N$ in time as $E(x,t)=\sum_{k=1}^N\sum_{i=1}^M E_h\varphi_i(x)\psi_k(t)$, where $E_h:=E_{h_{i,k}}$ denote unknown coefficients, substitute this expantion in variational formulation (5.6) with $v(x,t)=\varphi_j(x)\psi_l(t)$ and obtain following system of discrete equations

$$\begin{aligned}&-\sum_{k,l=1}^N\sum_{i,j=1}^M E_h\int_{\Omega_{FEM}}\varepsilon(x)\varphi_i(x)\varphi_j(x)\int_{t_{k-1}}^{t_{k+1}}\partial_t\psi_k(t)\partial_t\psi_l(t)\ dxdt\\&-\sum_{k,l=1}^N\sum_{i,j=1}^M E_h\int_{\Omega_{FEM}}\nabla\cdot\varphi_i(x)\nabla\cdot\varphi_j(x)\int_{t_{k-1}}^{t_{k+1}}\psi_k(t)\psi_l(t)\ dxdt\\&+\sum_{k,l=1}^N\sum_{i,j=1}^M E_h\int_{\partial\Omega}\varphi_i(x)\varphi_j(x)\int_{t_{k-1}}^{t_{k+1}}\partial_t\psi_k(t)\psi_l(t)\ dSdt\\&+\sum_{k,l=1}^N\sum_{i,j=1}^M E_h\int_{\Omega_{FEM}}\nabla\varphi_i(x)\nabla\varphi_j(x)\int_{t_{k-1}}^{t_{k+1}}\psi_k(t)\psi_l(t)\ dxdt\\&+s\sum_{k,l=1}^N\sum_{i,j=1}^M E_h\int_{\Omega_{FEM}}\nabla\cdot(\varepsilon\varphi_i(x))\nabla\cdot\varphi_j(x)\int_{t_{k-1}}^{t_{k+1}}\psi_k(t)\psi_l(t)\ dxdt\\&+\sum_{l=1}^N\sum_{j=1}^M\int_{\Omega_{FEM}}\int_{t_{k-1}}^{t_{k+1}}j(x)\varphi_j(x)\psi_l(t)\ dxdt=I_1+I_2+I_3+I_4+I_5+I_6=0.\end{aligned}\tag{5.7}$$

Next, we compute explicitly time integrals of (5.7) using the definition of piecewise linear functions in space and time, and get the linear system of equations:

$$\begin{aligned}M(\mathbf{E}^{k+1}-2\mathbf{E}^k+\mathbf{E}^{k-1})=&-\tau^2F^k+\tau^2D(\frac{1}{6}\mathbf{E}^{k-1}+\frac{2}{3}\mathbf{E}^k+\frac{1}{6}\mathbf{E}^{k+1})-\tau^2G(\frac{1}{6}\mathbf{E}^{k-1}+\frac{2}{3}\mathbf{E}^k+\frac{1}{6}\mathbf{E}^{k+1})\\&-s\tau^2C(\frac{1}{6}\mathbf{E}^{k-1}+\frac{2}{3}\mathbf{E}^k+\frac{1}{6}\mathbf{E}^{k+1})+\frac{1}{2}\tau M_{\partial\Omega}(\mathbf{E}^{k+1}-\mathbf{E}^{k-1}),\end{aligned}\tag{5.8}$$

with initial conditions $\mathbf{E}^0$ and $\mathbf{E}^1$ set to zero because of (5.2). Here, M and $M_{\partial\Omega}$ are the block mass matrices in space, D and C are the block stiffness matrix corresponding to the divergence terms, G is the stiffness matrix corresponding to the gradient term, F^k is the load vector at time level t_k corresponding to $j(\cdot,\cdot)$, whereas $\mathbf{E}^k$ denote the nodal values of $E(\cdot,t_k)$.

For example, to compute explicitly time integrals $\sum_{k,l=1}^N\int_{t_{k-1}}^{t_{k+1}}\partial_t\psi_k(t)\psi_l(t)dt$ in the term I_3, we use the definition of piecewise linear functions in time and observe that all terms in $\sum_{k,l=1}^N\int_{t_{k-1}}^{t_{k+1}}\partial_t\psi_k(t)\psi_l(t)dt$ are zeros unless $l=k-1,l=k,l=k+1$. Thus we have to compute only integrals

$$\int_{t_{k-1}}^{t_{k+1}}\partial_t\psi_{k-1}\psi_k dt,\int_{t_{k-1}}^{t_{k+1}}\partial_t\psi_{k+1}\psi_k dt,\int_{t_{k-1}}^{t_{k+1}}\partial_t\psi_k\psi_k dt.$$

To do that we have

$$
\begin{aligned}
\int_{t_{k-1}}^{t_{k+1}} \partial_t \psi_{k-1}\psi_k dt &= \int_{t_{k-1}}^{t_k} \partial_t \psi_{k-1}\psi_k dt + \int_{t_k}^{t_{k+1}} \partial_t \psi_{k-1}\psi_k dt = \int_{t_{k-1}}^{t_k} \partial_t \psi_{k-1}\psi_k dt \\
&= -\frac{1}{\tau}\int_{t_{k-1}}^{t_k} \frac{t-t_{k-1}}{t_k-t_{k-1}} dt = -\frac{1}{2}, \\
\int_{t_{k-1}}^{t_{k+1}} \partial_t \psi_{k+1}\psi_l dt &= \int_{t_{k-1}}^{t_k} \partial_t \psi_{k+1}\psi_k dt + \int_{t_k}^{t_{k+1}} \partial_t \psi_{k+1}\psi_k dt = \int_{t_k}^{t_{k+1}} \partial_t \psi_{k+1}\psi_k dt \\
&= -\frac{1}{\tau}\int_{t_k}^{t_{k+1}} \frac{t_{k+1}-t}{t_{k+1}-t_k} dt = \frac{1}{2}, \\
\int_{t_{k-1}}^{t_{k+1}} \partial_t \psi_k\psi_k dt &= \int_{t_{k-1}}^{t_k} \partial_t \psi_k\psi_k dt + \int_{t_k}^{t_{k+1}} \partial_t \psi_k\psi_k dt \\
&= \frac{1}{\tau}\int_{t_{k-1}}^{t_k} \frac{t-t_{k-1}}{t_k-t_{k-1}} dt - \frac{1}{\tau}\int_{t_{k-1}}^{t_k} \frac{t_{k+1}-t}{t_{k+1}-t_k} dt = 0.
\end{aligned}
\tag{5.9}
$$

By replacing in I_3 integrals $\sum_{k,l=1}^{N}\int_{t_{k-1}}^{t_{k+1}} \partial_t\psi_k(t)\psi_l(t)dt$ with their explicit expression through (5.9) we get the term $\frac{1}{2}(\mathbf{E}^{k+1}-\mathbf{E}^{k-1})$ in the last term of (5.8). In a similar way we obtain the term $\tau(\frac{1}{6}\mathbf{E}^{k-1}+\frac{2}{3}\mathbf{E}^{k}+\frac{1}{6}\mathbf{E}^{k+1})$ in (5.8) which corresponds to the the explicitly computed terms of the mass matrix in time $\sum_{k,l=1}^{N}\int_{t_{k-1}}^{t_{k+1}} \psi_k(t)\psi_l(t)dt$. Additional τ at the right hand side of (5.8) appears after the explicit computing of the time integrals $\sum_{k,l=1}^{N}\int_{t_{k-1}}^{t_{k+1}} \partial_t\psi_k(t)\partial_t\psi_l(t)dt$. This gives also terms $\mathbf{E}^{k+1}-2\mathbf{E}^{k}+\mathbf{E}^{k-1}$ at the left hand side of (5.8).

At the element level the matrix entries in (5.8) are explicitly given by:

$$
\begin{aligned}
M^e_{i,j} &= (\varepsilon\ \varphi_i, \varphi_j)_e, && (5.10)\\
M^{\partial\Omega}_{i,j} &= (\varphi_i, \varphi_j)_{\partial\Omega_{ij}}, && (5.11)\\
D^e_{i,j} &= (\ \nabla\cdot\varphi_i, \nabla\cdot\varphi_j)_e, && (5.12)\\
G^e_{i,j} &= (\ \nabla\varphi_i, \nabla\varphi_j)_e, && (5.13)\\
C^e_{i,j} &= (\ \nabla\cdot(\varepsilon\varphi_i), \nabla\cdot\varphi_j)_e, && (5.14)\\
F^e_{j,m} &= (j, \varphi_j)_e. && (5.15)
\end{aligned}
$$

To obtain an explicit scheme we approximate M by the lumped mass matrix M^L in space, i.e., the diagonal approximation obtained by taking the row sum of M [11, 15], as well as we use mass lumping in time by replacing terms corresponding to mass matrix in time $\frac{1}{6}\mathbf{E}^{k-1}+\frac{2}{3}\mathbf{E}^{k}+\frac{1}{6}\mathbf{E}^{k+1}$ by $\mathbf{E}^k$.

Next, by multiplying (5.8) with $(M^L)^{-1}$, we obtain the following fully explicit time stepping method to solve (3.13)-(3.16):

$$
\begin{aligned}
\mathbf{E}^{k+1}(1-\frac{1}{2}\tau M^{\partial\Omega}(M^L)^{-1}) &= -\tau^2(M^L)^{-1}F^k + 2\mathbf{E}^k + \tau^2(M^L)^{-1}D\mathbf{E}^k - \tau^2(M^L)^{-1}G\mathbf{E}^k \\
&\quad - s\tau^2(M^L)^{-1}C\mathbf{E}^k - (1+\frac{1}{2}\tau M^{\partial\Omega}(M^L)^{-1})\mathbf{E}^{k-1}.
\end{aligned}
\tag{5.16}
$$

In the case when (5.16) is used only in Ω_{FEM} in the hybrid FEM/FDM method, it reduces to the following scheme

$$
\begin{aligned}
\mathbf{E}^{k+1} &= -\tau^2(M^L)^{-1}F^k + 2\mathbf{E}^k + \tau^2(M^L)^{-1}D\mathbf{E}^k - \tau^2(M^L)^{-1}G\mathbf{E}^k \\
&\quad - s\tau^2(M^L)^{-1}C\mathbf{E}^k - \mathbf{E}^{k-1}.
\end{aligned}
\tag{5.17}
$$

5.2. Finite difference formulation. We recall (see section 3) that in Ω_{FDM} we have $\varepsilon(x) = \mu(x) = 1$. Thus in Ω_{FDM} we have to solve system of vector wave equations for the vector field $E = (E_1, E_2, E_3)$

$$\partial_t^2 E - \Delta E = -j \tag{5.18}$$

$$E(x,0) = 0, \quad E_t(x,0) = 0 \text{ in } \Omega, \tag{5.19}$$

$$\partial_n E(x,t) = -\partial_t E(x,t) \text{ on } \partial\Omega_T. \tag{5.20}$$

Using standard finite difference discretization of the equation (5.18) in Ω_{FDM} we obtain following explicit scheme

$$E_{i,j,m}^{k+1} = -\tau^2 j_{i,j,m}^k + \tau^2 \Delta E_{i,j,m}^k + 2E_{i,j,m}^k - E_{i,j,m}^{k-1}, \tag{5.21}$$

where $E_{i,j,m}^k$ is the solution on the time iteration k at the discrete point (i,j,m), $j_{i,j,m}^k$ is the discrete analog of the function j, τ is the time step, and $\Delta E_{i,j,m}^k$ is the discrete Laplacian. In three dimensions, to approximate $\Delta E_{i,j,m}^k$ we get the standard seven-point stencil:

$$\Delta E_{i,j,m}^k = \frac{E_{i+1,j,m}^k - 2E_{i,j,m}^k + E_{i-1,j,m}^k}{dx^2} + \frac{E_{i,j+1,m}^k - 2E_{i,j,m}^k + E_{i,j-1,m}^k}{dy^2} + \frac{E_{i,j,m+1}^k - 2E_{i,j,m}^k + E_{i,j,m-1}^k}{dz^2}, \tag{5.22}$$

where dx, dy, and dz are the steps of the discrete finite difference meshes in the directions x, y, z, respectively.

5.3. Absorbing boundary conditions. To discretize absorbing boundary condition (5.20) in Ω_{FDM} we use forward finite difference approximation in the middle point, which gives a numerical approximation of higher order than ordinary (backward or forward) finite difference approximation. For example, for the left boundary of Ω_{FDM} we have following variant of the condition (5.20)

$$\frac{\partial E(x,t)}{\partial x} = \frac{\partial E(x,t)}{\partial t}$$

Then we use the following finite difference discretization of the above equation

$$\frac{E_{i,j,m}^{k+1} - E_{i,j,m}^k}{dt} + \frac{E_{i+1,j,m}^{k+1} - E_{i+1,j,m}^k}{dt} - \frac{E_{i+1,j,m}^k - E_{i,j,m}^k}{dx} - \frac{E_{i+1,j,m}^{k+1} - E_{i,j,m}^{k+1}}{dx} = 0, \tag{5.23}$$

which can be transformed to

$$E_{i,j,m}^{k+1} = E_{i+1,j,m}^k + E_{i,j,m}^k \frac{dx - dt}{dx + dt} - E_{i+1,j,m}^{k+1} \frac{dx - dt}{dx + dt}. \tag{5.24}$$

For other boundaries of the Ω_{FDM} boundary condition (5.20) can be written similarly.

6. The domain decomposition FEM/FDM method. We now describe the data communication for solution of the problem (3.13)-(3.14) between the finite element method on the unstructured part of the mesh, Ω_{FEM}, and the finite difference method on the structured part, Ω_{FDM}. This communication is achieved by mesh overlapping across a two-element thick layer around Ω_{FEM} - see Figure 3.1.

First, using the Figure 3.1 we observe that the interior nodes of the computational domain Ω belong to either of the following sets:

ω_o Nodes 'o' interior to Ω_{FDM} that lie on the boundary of Ω_{FEM},
$\omega_\times$ Nodes '$\times$' interior to Ω_{FEM} that lie on the boundary of Ω_{FDM},
ω_* Nodes '$*$' interior to Ω_{FEM} that are not contained in Ω_{FDM},
ω_D Nodes 'D' interior to Ω_{FDM} that are not contained in Ω_{FEM}.

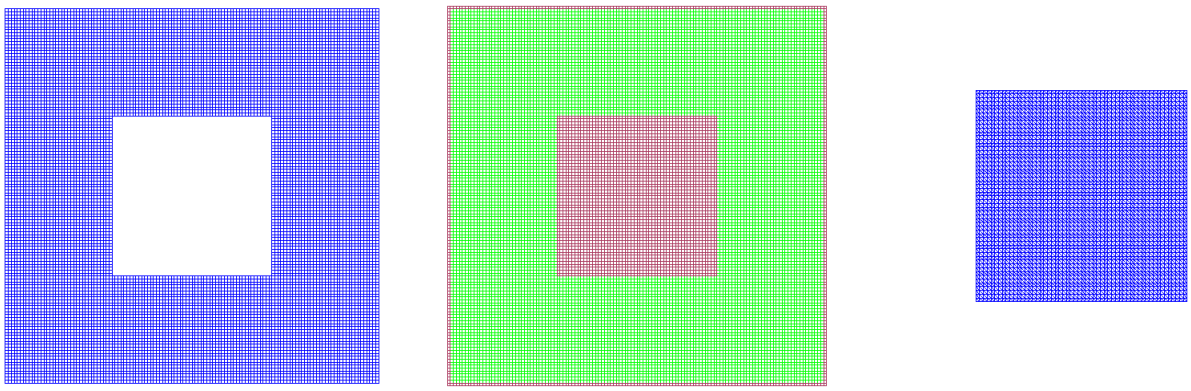

(a) Ω_{FDM} (b) $\Omega = \Omega_{FEM} \cup \Omega_{FDM}$ (c) Ω_{FEM}

Fig. 7.1: *The hybrid mesh (b) is a combinations of a structured mesh (a), where FDM is applied, and a mesh (c), where we use FEM, with a two layers overlapping of structured elements. The coefficient $\varepsilon(x)$ in (5.1) is given as follows: $\varepsilon(x) = 1$ in Ω_{FDM} and $\varepsilon(x) \geq 1$ for $x \in \Omega \setminus \Omega_{FDM}$.*

We also note that because of using explicit domain decomposition FEM/FDM method we need to choose time step τ such that the whole scheme remains stable. We use the stability analysis on the structured meshes and choose the largest time step in our computations accordingly to the stability condition

$$\tau \leq \frac{\sqrt{\varepsilon\mu}}{\sqrt{\frac{1}{dx^2} + \frac{1}{dy^2} + \frac{1}{dz^2}}}. \tag{6.1}$$

Usually, we have $dx = dy = dz = h$, and the condition (6.1) can be rewritten as

$$\tau \leq h\sqrt{\frac{\varepsilon\mu}{3}}. \tag{6.2}$$

Algorithm.
At every time step we perform the following operations:

1. On the structured part of the mesh Ω_{FDM} compute E^{k+1} from (5.21) with absorbing boundary condition (5.20) at $\partial\Omega$, with E^k and E^{k-1} known.
2. On the unstructured part of the mesh Ω_{FEM} compute E^{k+1} by using the explicit finite element scheme (5.17) with E^k and E^{k-1} known.
3. Use the values of the electric field E^{k+1} at nodes $\omega_\times$, which are computed using the finite element scheme (5.17), as a boundary condition for the finite difference method in Ω_{FDM}.
4. Use the values of the electric field E^{k+1} at nodes ω_o, which are computed using the finite difference scheme (5.21), as a boundary condition for the finite element method in Ω_{FEM}.
5. Apply swap of the solutions for the electric field to be able perform algorithm on a new time level k.

7. Numerical Studies. In all our tests we choose the computational domain $\Omega = [-8.0, 8.0] \times [-8.0, 8.0]$. This domain is split into a finite element subdomain $\Omega_{FEM} = [-3.5, 3.5] \times [-3.5, 3.5]$ and a surrounding region Ω_{FDM} with a structured mesh, $\Omega = \Omega_{FEM} \cup \Omega_{FDM}$, see Figure 7.1.

The spatial mesh in Ω consists of triangles and in Ω_{FDM} - of squares. The boundary of the domain Ω is $\partial\Omega = \partial\Omega_1 \cup \partial\Omega_2 \cup \partial\Omega_3$. Here, $\partial\Omega_1$ and $\partial\Omega_2$ are the top and the bottom sides of the Ω, and $\partial\Omega_3$ is the union of the left and right sides of this domain, see Figure 7.1. Let us define $\Omega_{FEM_T} := \Omega_{FEM} \times (0, T)$, $\Omega_{FDM_T} := \Omega_{FDM} \times (0, T)$.

We also denote different boundaries in the domain decomposition method (see section (6) for details) as follows: boundary of the Ω_{FEM} we define by $\partial\Omega_{FEM}$, outer boundary of the Ω_{FDM} we define by $\partial\Omega$, inner boundary of the Ω_{FDM} we define by $\partial\Omega_{FDM}$, nodes corresponding to $\partial\Omega_{FEM}$ but which lies in Ω_{FDM}, we define by $\partial\Omega_{\omega_0}$, and nodes corresponding to $\partial\Omega_{FDM}$ but which lies in Ω_{FEM}, we define by $\partial\Omega_{\omega_x}$. Next, let $\partial\Omega_{FDM_T} := \partial\Omega_{FDM}\times(0,T)$, $\partial\Omega_{FEM_T} := \partial\Omega_{FEM}\times(0,T)$, $\partial\Omega_{\omega_{xT}} := \partial\Omega_{\omega_x}\times(0,T)$, $\partial\Omega_{\omega_{0T}} := \partial\Omega_{\omega_0}\times(0,T)$.

7.1. Numerical studies with exact smooth solution. In the tests of this section we solve the problem (5.1)-(5.3) in Ω in time $T=[0,20]$ in two dimensions with the known smooth solution

$$\begin{aligned} E_1(x,y,t) &= \frac{t^2}{2.0}\cos(\pi x)\cdot\sin(\pi y),\\ E_2(x,y,t) &= -\frac{t^2}{2.0}\sin(\pi x)\cdot\cos(\pi y). \end{aligned} \tag{7.1}$$

In this case the problem (5.1)-(5.3) for the electric field in Ω_{FEM} reduces to the following problem in two dimensions

$$\varepsilon\frac{\partial^2 E_1}{\partial t^2}+\frac{\partial}{\partial y}\Big(\frac{\partial E_2}{\partial x}-\frac{\partial E_1}{\partial y}\Big)=\cos(\pi x)\cdot\sin(\pi y)(\varepsilon+t^2\pi^2),\ \text{in}\quad \text{in } \Omega_{FEM_T}, \tag{7.2}$$

$$\varepsilon\frac{\partial^2 E_2}{\partial t^2}-\frac{\partial}{\partial x}\Big(\frac{\partial E_2}{\partial x}-\frac{\partial E_1}{\partial y}\Big)=\sin(\pi x)\cdot\cos(\pi y)(-\varepsilon-t^2\pi^2),\ \text{in}\ \ \Omega_{FEM_T}, \tag{7.3}$$

$$E(x,0)=0,\quad E_t(x,0)=0 \text{ in } \ \Omega_{FEM}, \tag{7.4}$$

$$E(x,t)_{\partial\Omega_{FEM_T}}=E(x,t)_{\partial\Omega_{\omega_{0T}}}. \tag{7.5}$$

In Ω_{FDM} our coefficients are $\varepsilon=\mu=1$, and in this domain we have to solve the following problem

$$\begin{aligned} \partial_{tt}E_1-\triangle E_1 &= \cos(\pi x)\cdot\sin(\pi y)(\varepsilon+t^2\pi^2),\quad \text{in } \Omega_{FDM_T},\\ \partial_{tt}E_2-\triangle E_2 &= \sin(\pi x)\cdot\cos(\pi y)(-\varepsilon-t^2\pi^2) \text{ in } \ \Omega_{FDM_T},\\ E(x,0) &= 0,\ E_t(x,0)=0,\ \text{in } \Omega_{FDM},\\ E(x,t)_{\partial\Omega_{FDM_T}} &= E(x,t)_{\partial\Omega_{\omega_{xT}}},\\ \partial_n E\big|_{\partial\Omega} &= -\partial_t u \text{ on } \partial\Omega_T. \end{aligned} \tag{7.6}$$

We choose the time step $\tau=0.02$ correspondingly to the CFL condition (6.2), while the penalty factor is always set to $s=1$.

7.1.1. Test 1. In this test we use the domain decomposition method with the coefficient ε defined as a function inside Ω_{FEM} such that

$$\varepsilon(x)=\begin{cases} 1+A(\sin(\frac{\pi}{3}x))^2\cdot(\sin(\pi/3)y)^2, & 0\le x\le 3,\quad \text{and}\quad -3\le y\le 0;\\ 1, & \text{at all other points}\quad , \end{cases} \tag{7.7}$$

with values of the amplitude $A=3,12,26,37,51$, see Figure 7.2-a) for this function in the case when amplitude $A=3$ in (7.7).

First we perform computations on the mesh with the mesh size $h=0.125$. Figures 7.3 demonstrate the continuity of the computed components of the vector field (E_1,E_2) across the Finite Difference/Finite Element mesh in the domain decomposition method with $A=3$ in (7.7) at different times. We observe that the components of the vector field (E_1,E_2) remains smooth across the FE/FD interface at all times. We also observe that the exact components of the vector field looks very similar to the computed one - compare Figures 7.3.

Figures 7.4 show the vector field (E_1,E_2) of the computed solution in the domain decomposition method compared with the exact one at different times. We observe the smoothness of the vector field when computing with $A=3$ in (7.7). Figure 7.9 show the time evolution of the intensity of the exact electric field

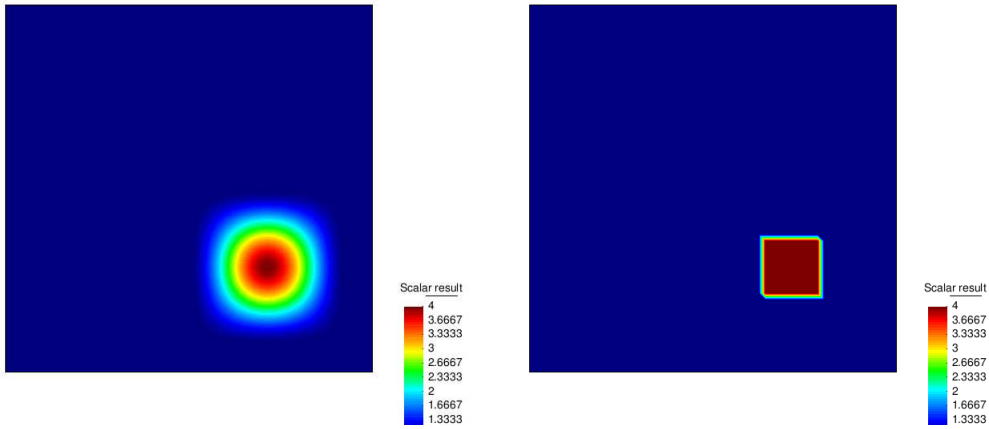

a) $\max \varepsilon = 4$ in Test 1 b) $\varepsilon = 4$ in Test 2

Fig. 7.2: *Coefficient ε in different tests.*

$|E| = \sqrt{E_1^2 + E_2^2}$ compared with the simulated solution $|E_h| = \sqrt{{E_h}_1^2 + {E_h}_2^2}$. The solution is presented at different points of the computational domain Ω_{FEM}. The Figure 7.10-a) shows corresponding to the Figure 7.9 computed relative L_2-norms in Ω_{FEM} in the time $T = (0, 20)$. Relative L_2 norms are defined as $\frac{||E-E_h||_{L_2(\Omega_{FEM})}}{||E||_{L_2(\Omega_{FEM})}}$, where E and E_h are the exact and the computed intensities of the electric fields, correspondingly. Figure 7.10-b) shows the computed L_2-norms of $E - E_h$ in Ω_{FEM} in time $T = (0, 20)$. From the Figures 7.3-7.7,7.10 we can conclude that the computed solution E_h is very close to the exact one E as soon as values of the coefficient ε are not too big ($A < 26$ in (7.7)), and the final time T is also not very large ($T < 10$).

Let us compare Figure 7.8 with the Figure 7.7. On the Figure 7.7 we observe appearance of the spurious modes when computing the domain decomposition method on the mesh with the mesh size $h = 0.125$, with large times ($T > 8$) and with big values of the amplitude $A > 12$ in (7.7). However, these spurious solutions are removed as mesh is refined, see Figure 7.8.

7.1.2. Test 2. In this test we use the domain decomposition method when $\varepsilon = 1$ in Ω except one small square in Ω_{FEM}, where $\varepsilon = A$ with $A = 3, 12, 26, 37, 51$, see Figure 7.2-b) for example of this coefficient in the case when $\varepsilon = 4$ inside the small square. In other words, the coefficient ε is defined inside Ω_{FEM} as

$$\varepsilon(x) = \begin{cases} 1 + A, & 0 \le x \le 3, \quad \text{and} \quad -3 \le y \le 0; \\ 1, & \text{at all other points} \quad , \end{cases} \tag{7.8}$$

with values of the amplitude $A = 3, 12, 26, 37, 51$.

In this case we have similar behaviour of the electric field as in the Test 1 even in the presence of the discontinuity of the coefficient ε in the model equations. In all cases of this test we have continuity of the computed solution across FEM/FDM mesh, and behaviour of it is very similar to the behaviour of the solution presented at all Figures related to the Test 1, and thus, we do not present these solutions again. From this test we can conclude that the computed solution E_h on the mesh with the mesh size $h = 0.125$ is very close to the exact one solution E as soon as discontinuity in the coefficient ε is not big ($\varepsilon < 26$) and the computational time T is not very large ($T < 10$). However, when mesh is refined these spurious solutions disappear even when computing the model problem with big values of the amplitude A in small square in Ω_{FEM}.

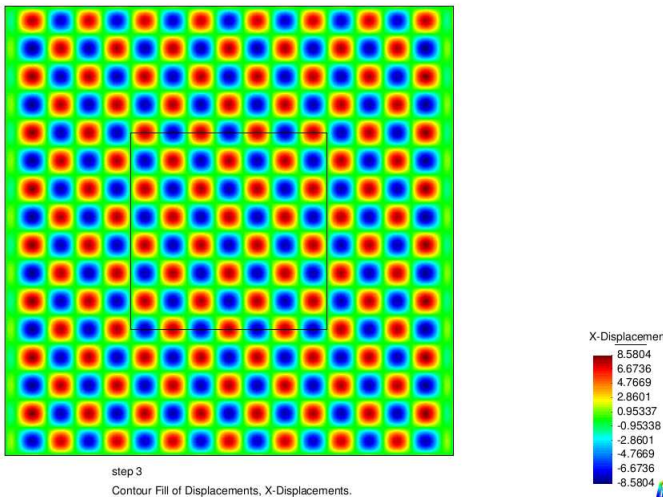

a) E_1 in Ω

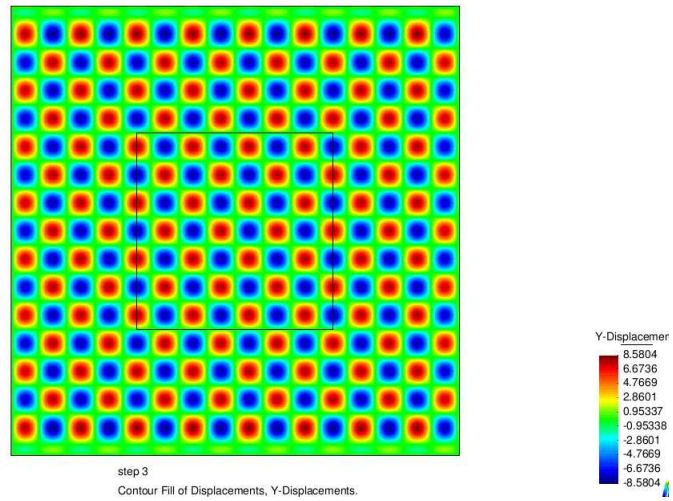

b) E_2 in Ω

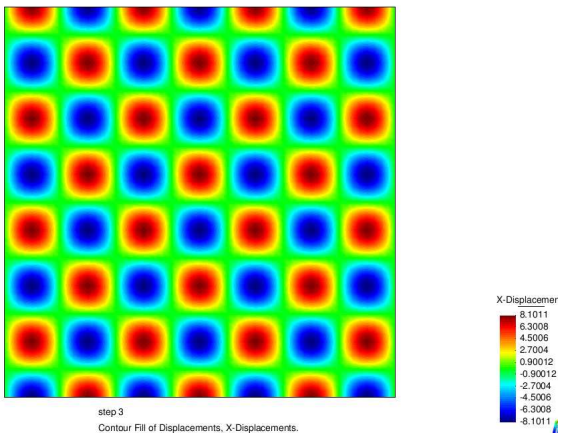

c) E_1 in Ω_{FEM}

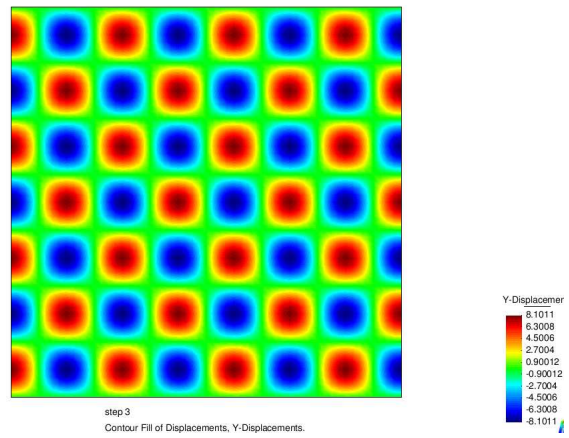

d) E_2 in Ω_{FEM}

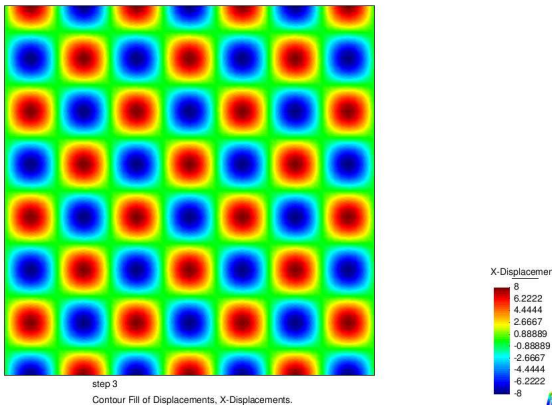

e) E_1 analytic in Ω_{FEM}

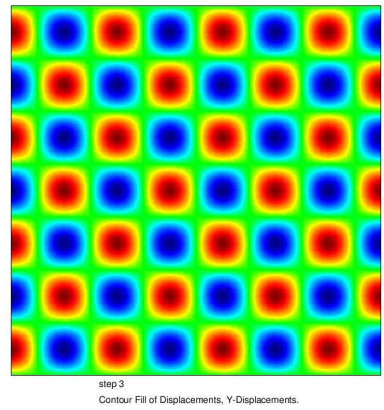

f) E_2 analytic in Ω_{FEM}

Fig. 7.3: *Test 1. Comparison of the components* (E_1, E_2) *in the analytic and the computed solution for* $A = 3$ *in the domain decomposition FEM/FDM method at time moment* $t = 8.0$*. We present at (a), (b) components* E_1, E_2 *in* Ω*; at (c), (d) components* E_1, E_2 *of the finite element solution in* Ω_{FEM}*; and at (e), (f) components* E_1, E_2 *of the analytic solution in* Ω_{FEM}*.*

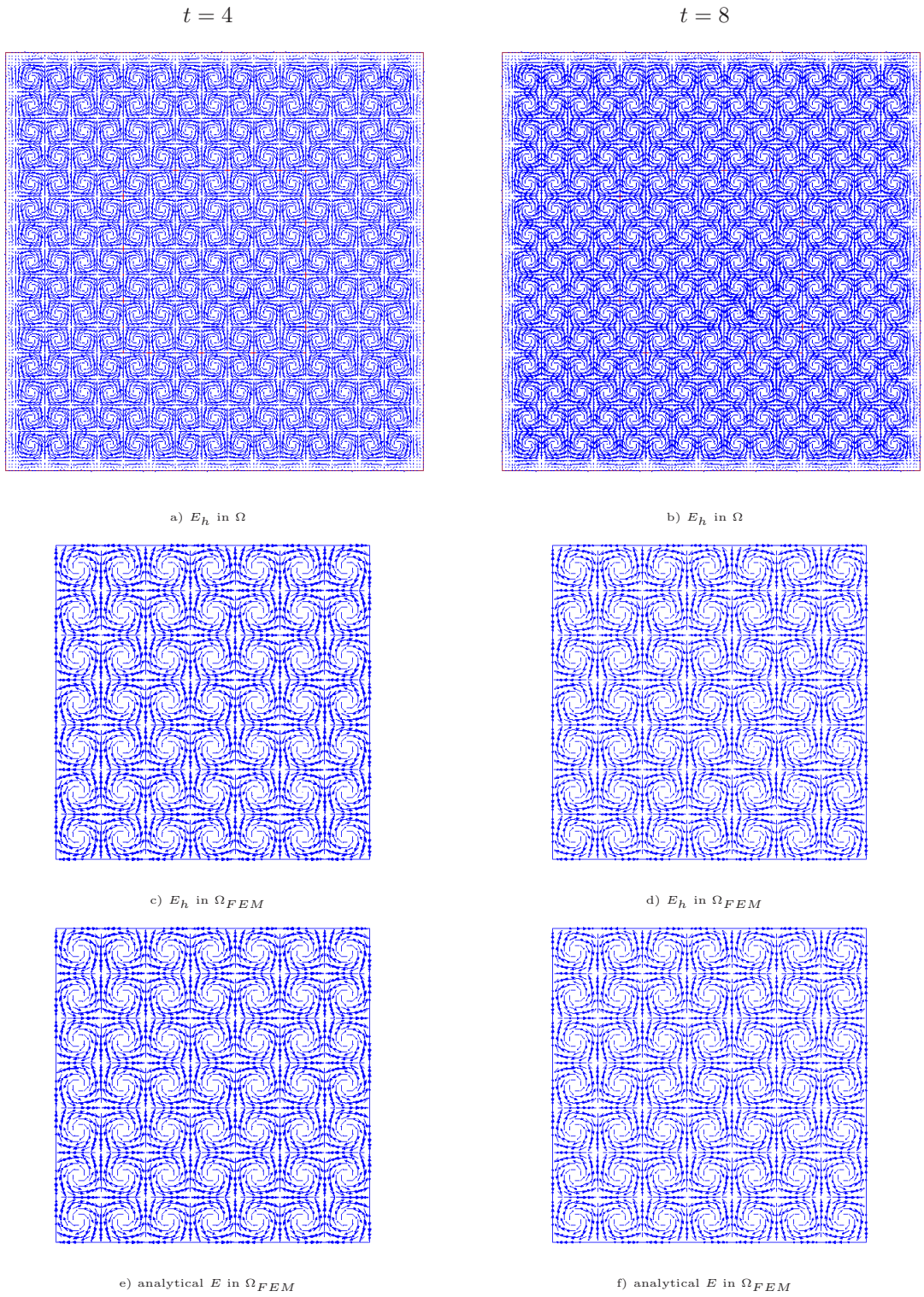

Fig. 7.4: *Test 1. Behaviour of the computed vector electrical field $E_h = (E_{1h}, E_{2h})$ and analytical one in the domain decomposition FEM/FDM method at time moments $t = 4.0$ and $t = 8$. We show the electrical vector field on: a),b) in the domain decomposition FEM/FDM method in Ω; on c),d) in Ω_{FEM} and on e),f) analytical vector field $E = (E_1, E_2)$ in Ω_{FEM}.*

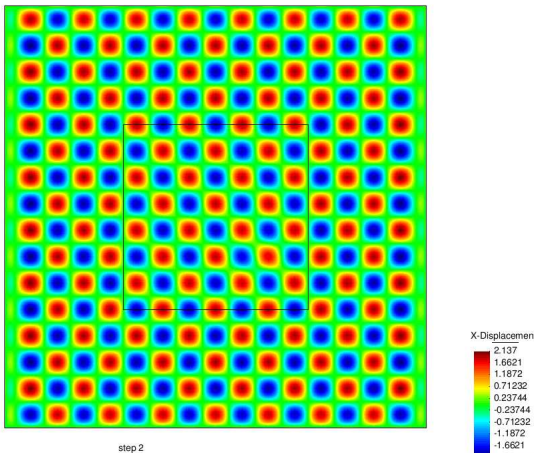

a) $A = 12$, E_1 in Ω

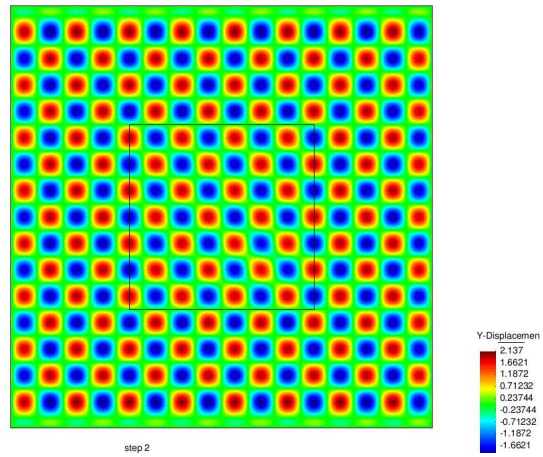

b) $A = 12$, E_2 in Ω

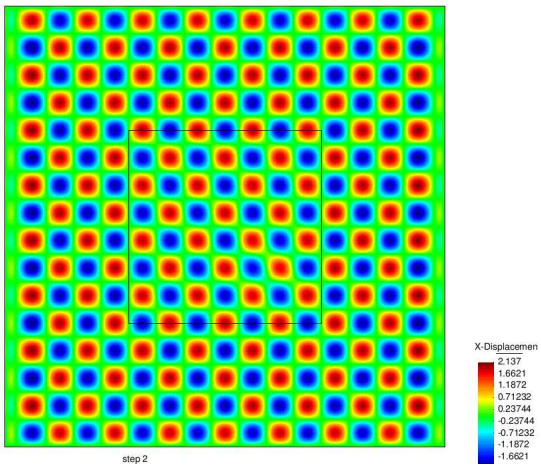

c) $A = 26$, E_1 in Ω

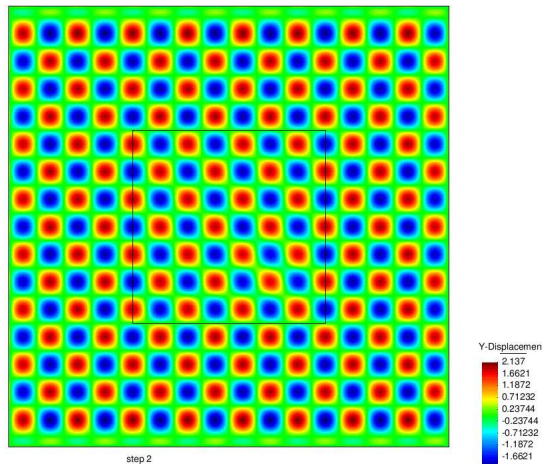

d) $A = 26$, E_2 in Ω

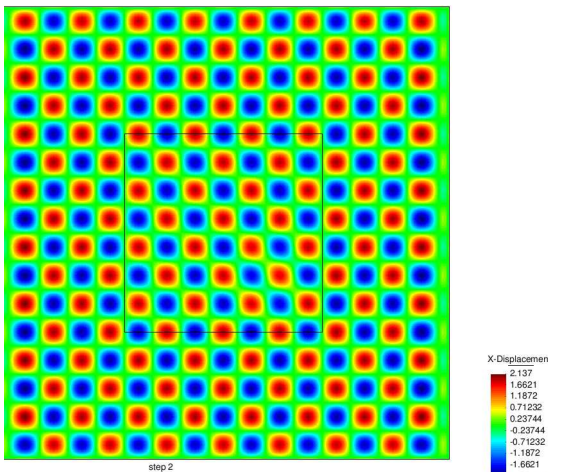

e) $A = 51$, E_1 in Ω_{FEM}

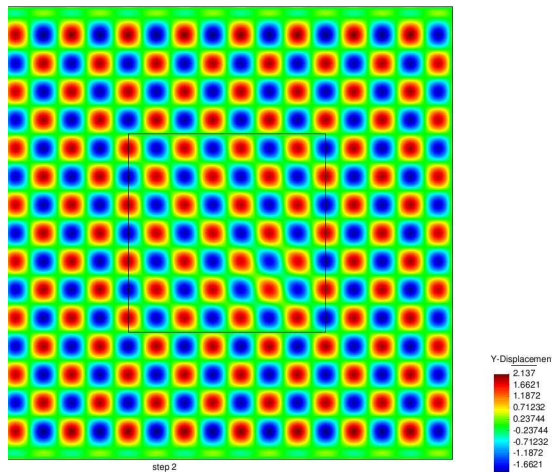

f) $A = 51$, E_2 in Ω_{FEM}

Fig. 7.5: *Test 1. Computed solutions in the domain decomposition FEM/FDM method at time moment* $t = 4.0$ *in* Ω*. We show comparison of the computed solutions with different values of the coefficient* ε *inside* Ω_{FEM} *in Maxwell equations. On a),b) the amplitude* $A = 26$ *for coefficient* ε *in (7.7), and on c),d)* $A = 51$ *in (7.7).*

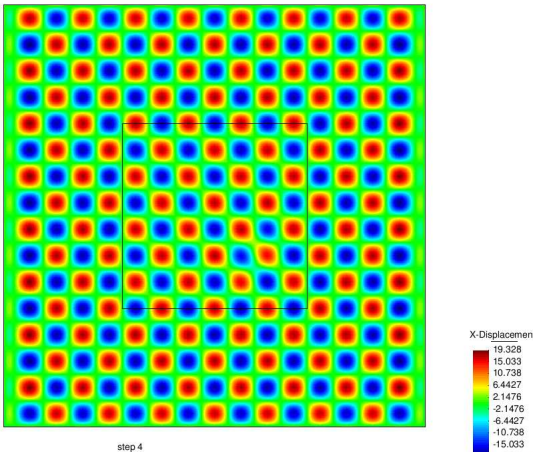

a) $A = 12$, E_1 in Ω

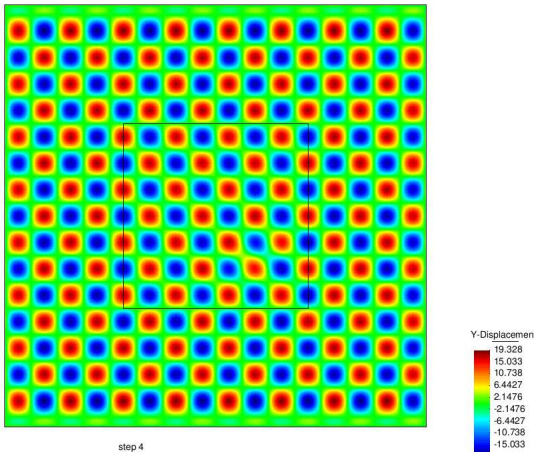

b) $A = 12$, E_2 in Ω

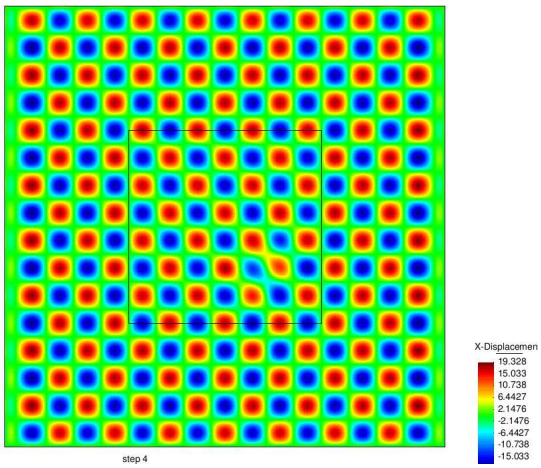

c) $A = 26$, E_1 in Ω

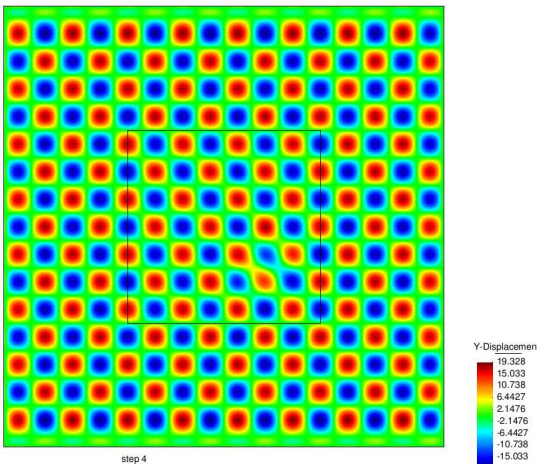

d) $A = 26$, E_2 in Ω

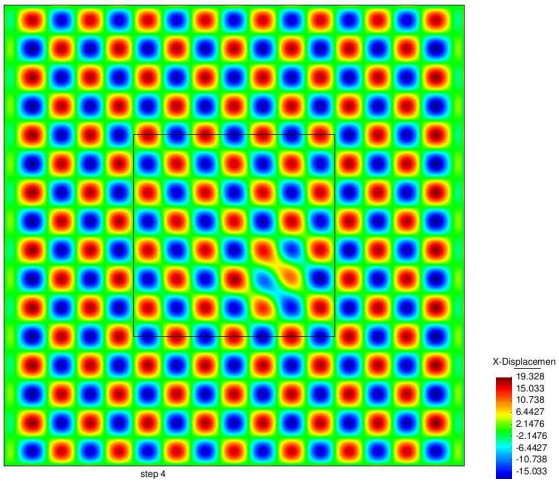

e) $A = 51$, E_1 in Ω_{FEM}

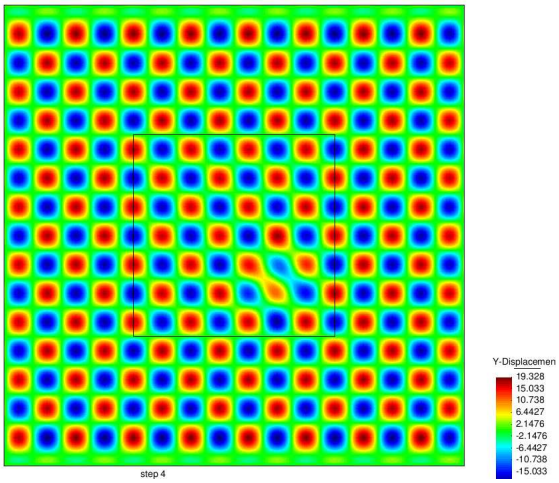

f) $A = 51$, E_2 in Ω_{FEM}

Fig. 7.6: *Test 1. Computed solutions in the domain decomposition FEM/FDM method at time moment* $t = 8.0$ *in* Ω*. We show comparison of the computed solutions with different values of the coefficient* ε *inside* Ω_{FEM} *in Maxwell equations. On a),b) the amplitude* $A = 26$ *for coefficient* ε *in (7.7), and on c),d)* $A = 51$ *in (7.7).*

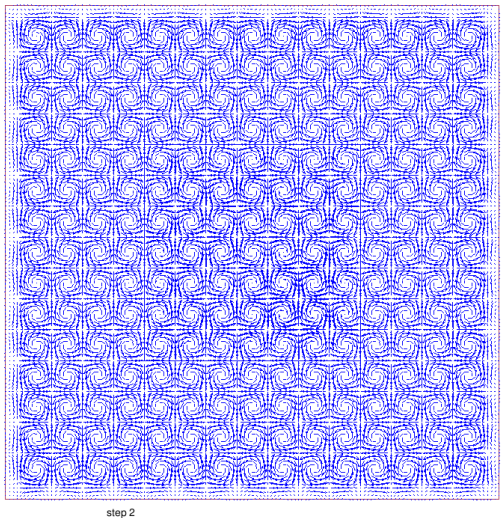

a) $A = 26, T = 4$

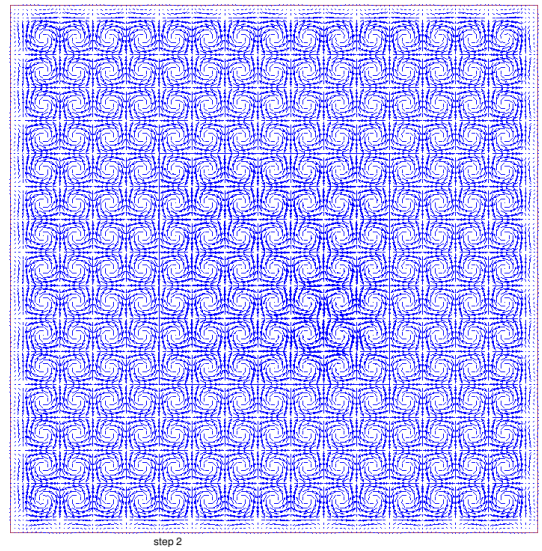

b) $A = 51, T = 4$

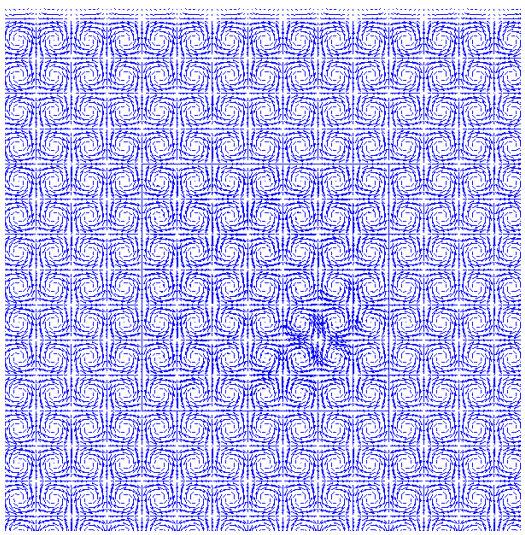

c) $A = 26, T = 8$

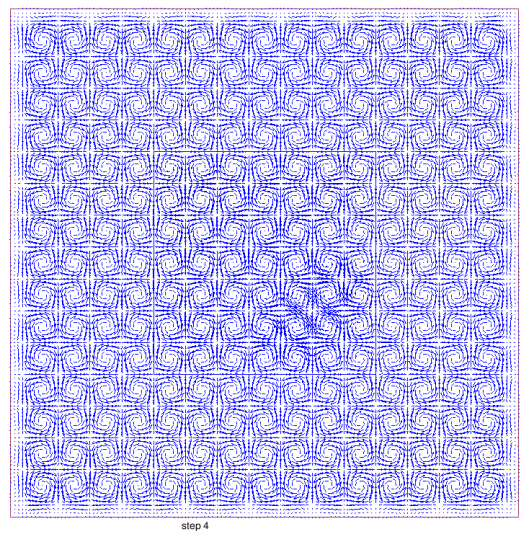

d) $A = 51, T = 8$

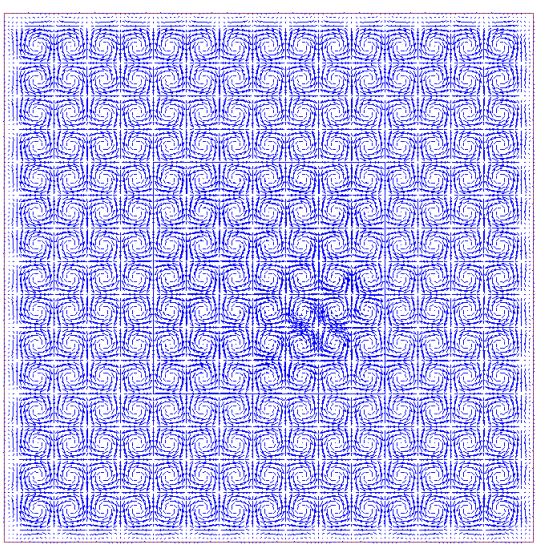

e) $A = 26, T = 20$

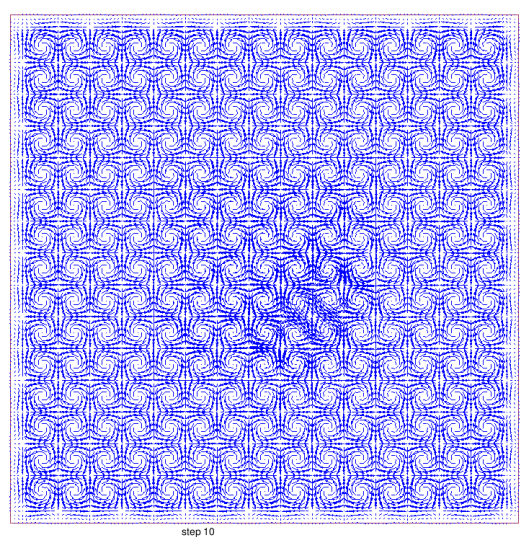

f) $A = 51, T = 20$

Fig. 7.7: *Test 1. Behaviour of the computed vector electrical field $E_h = (E_{1h}, E_{2h})$ in the domain decomposition FEM/FDM method in Ω at different time moments. We show the electrical vector field for different values of the amplitude A in (7.7) in Ω.*

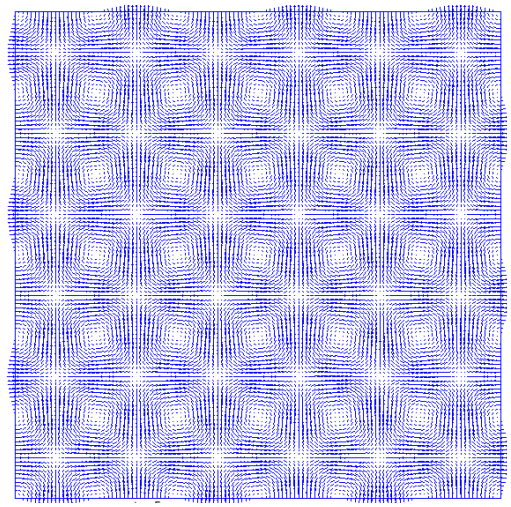

a) $A = 26, T = 20$

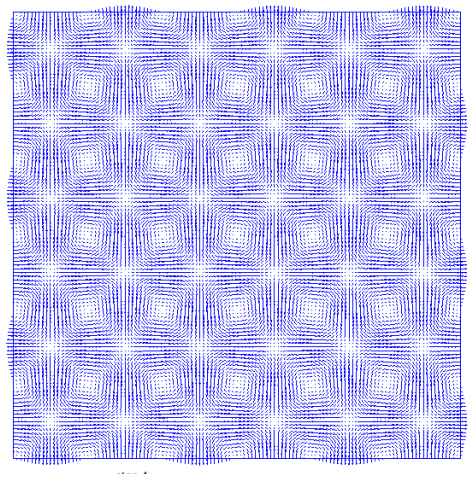

b) $A = 37, T = 20$

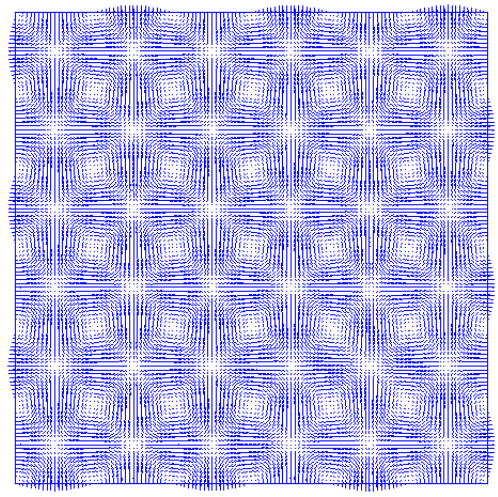

c) $A = 51, T = 20$

Fig. 7.8: *Test 1.Removable of spurious solutions on the finer mesh with the mesh size* $h = 0.05$. *We show behaviour of the computed vector electrical field* $E_h = (E_{1h}, E_{2h})$ *in the domain decomposition FEM/FDM method in* Ω_{FEM} *at* $T = 20$. *We present the electrical vector field for different values of the amplitude* A *in (7.7) in* Ω. *Compare with the Fig.7.7 where spurious modes appeared already at the time* $T = 8$ *where computations was performed on the coarser mesh with the mesh size* $h = 0.125$.

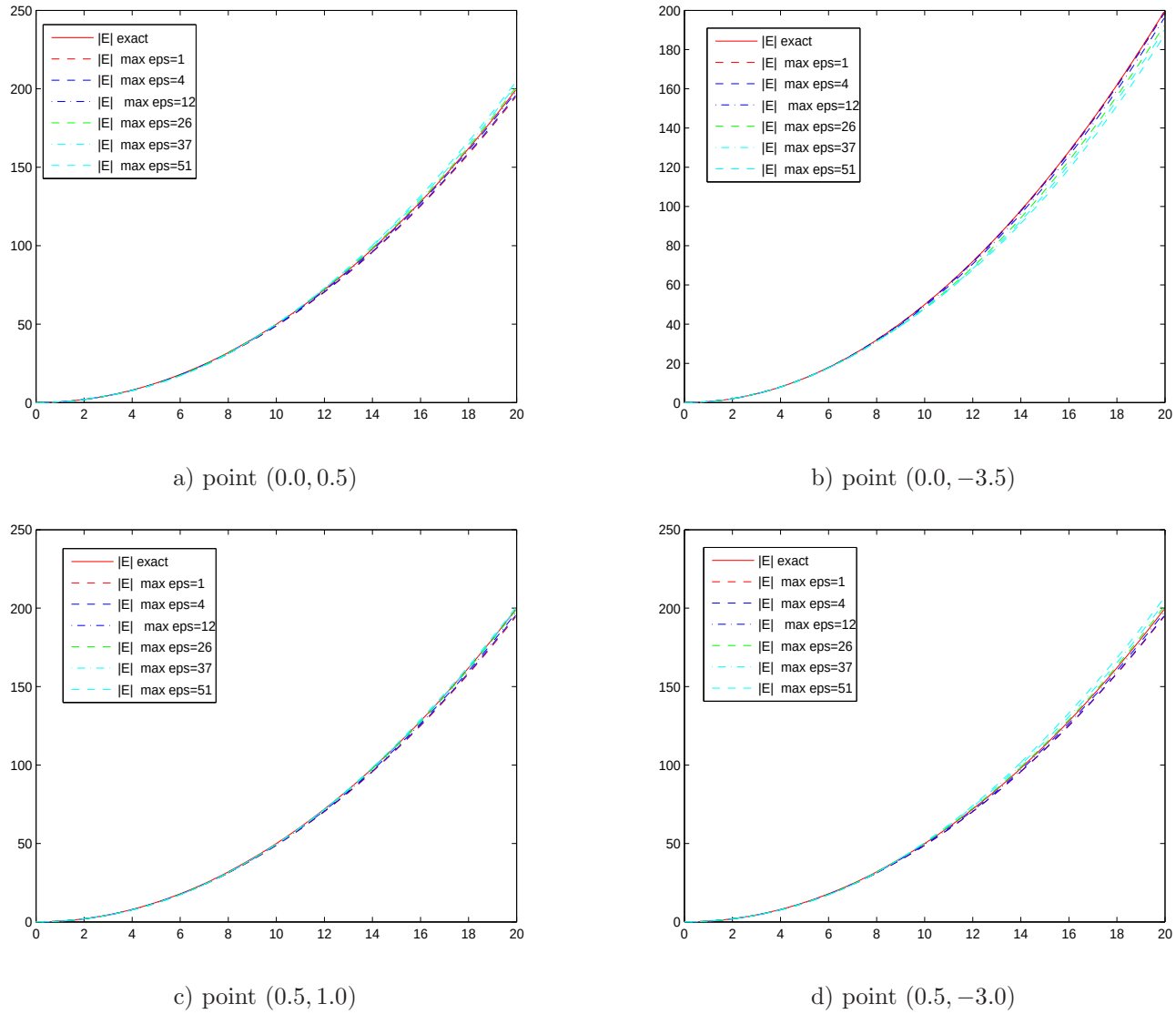

a) point $(0.0, 0.5)$

b) point $(0.0, -3.5)$

c) point $(0.5, 1.0)$

d) point $(0.5, -3.0)$

Fig. 7.9: *Test 1. Behaviour of* $E = \sqrt{E_1^2 + E_2^2}$ *in time* $T = (0, 20)$ *of the exact and computed solutions of equation (7.11)-(7.14): a) at the point* $(0.0, 0.5)$*, which is located in the center of the computational domain* Ω_{FEM}*; b) at the point* $(0.0, -3.5)$*, which is located at the bottom boundary of the* Ω_{FEM}*; c) at the point* $(0.5, 1.0)$*, which is located close to the center of the* Ω_{FEM}*; d) at the point* $(0.5, -3.0)$*, which is located at the lower part of the* Ω_{FEM}*. We show comparison of solutions with values of the amplitude* $A = 4, 12, 26, 37, 51$ *in (7.7). Here the horizontal axis denotes the computational time.*

7.2. Numerical studies with a plane wave. In the tests of this section we solve the problem (5.1)-(5.3) in Ω in time $T = [0, 20]$ in two dimensions with the plane wave $f(t)$ defined as

$$f(t) = \begin{cases} \sin(\omega t), & \text{if } t \in \left(0, \frac{2\pi}{\omega}\right), \\ 0, & \text{if } t > \frac{2\pi}{\omega}. \end{cases} \tag{7.9}$$

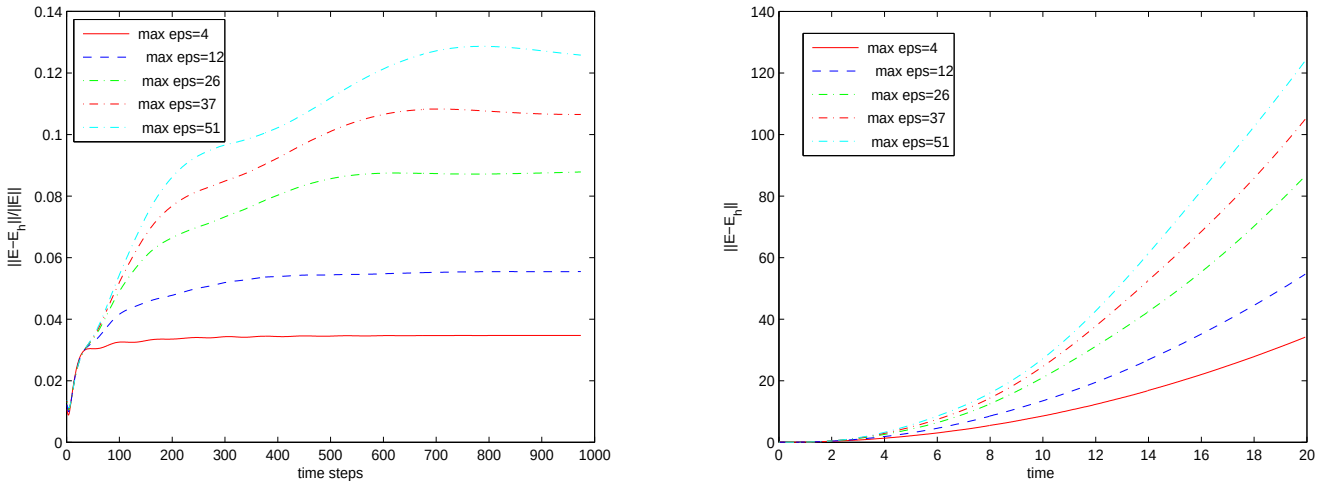

a) b)

Fig. 7.10: *Test 1. a) Relative errors* $\frac{||E-E_h||_{L_2\Omega_{FEM}}}{||E||_{L_2\Omega_{FEM}}}$ *in time* $T = (0, 20)$*; b) Norms* $||E - E_h||_{L_2\Omega_{FEM}}$ *in time* $T = (0, 20)$.

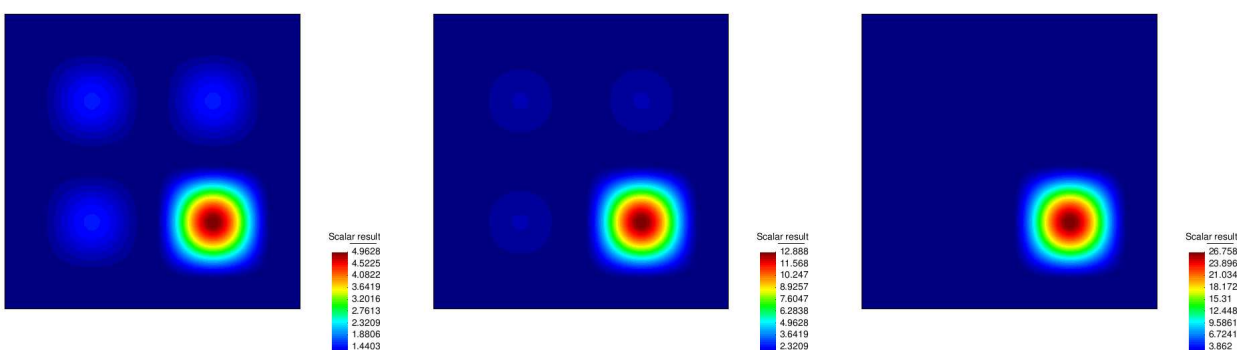

a) $A = 4$ b) $A = 12$ c) $A = 26$

Fig. 7.11: *Different coefficients* ε *defined by (7.17) used in tests with plane wave.*

In Ω_{FDM} our coefficients are $\varepsilon = \mu = 1$, and in this domain we have to solve the following problem

$$\begin{aligned} E_{tt} - \triangle E &= 0, && \text{in } G \times (0, T), \\ E(x, 0) &= 0, && \text{in } G, \\ E_t(x, 0) &= 0, && \text{in } G, \\ E_1 = 0, E_2(x, t) &= f(t), && \text{on } \partial\Omega_1 \times (0, t_1], \\ \partial_n E(x, t) &= -\partial_t u(x, t), && \text{on } \partial\Omega_1 \times (t_1, T), \\ \partial_n E(x, t) &= -\partial_t u(x, t), && \text{on } \partial\Omega_2 \times (0, T), \\ \partial_n u(x, t) &= 0, && \text{on } \partial G_3 \times (0, T), \end{aligned} \tag{7.10}$$

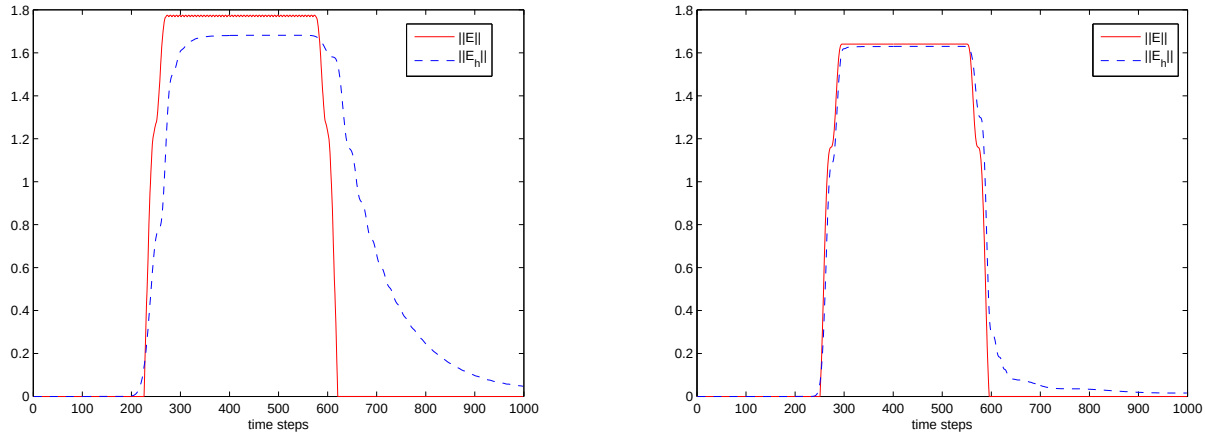

a) $h = 0.125$ b) $h = 0.05$

Fig. 7.12: *a) Test 3: numerical comparison of the computed L_2-norms for $||E||$ and $||E_h||$ on different meshes with mesh sizes $h = 0.05$ and $h = 0.125$ in time $T = (0, 20)$ in Ω_{FEM}. Here the horizontal axis denotes the the number of time steps in time $T = (0, 20)$.*

and in Ω_{FEM} we have to solve

$$\varepsilon \frac{\partial^2 E_1}{\partial t^2} + \frac{\partial}{\partial y}\Big(\frac{\partial E_2}{\partial x} - \frac{\partial E_1}{\partial y}\Big) = 0, \text{ in } \quad \text{ in } \Omega_{FEM_T}, \tag{7.11}$$

$$\varepsilon \frac{\partial^2 E_2}{\partial t^2} - \frac{\partial}{\partial x}\Big(\frac{\partial E_2}{\partial x} - \frac{\partial E_1}{\partial y}\Big) = 0, \text{ in } \ \Omega_{FEM_T}, \tag{7.12}$$

$$E(x,0) = 0, \quad E_t(x,0) = 0 \text{ in } \ \Omega_{FEM}, \tag{7.13}$$

$$E(x,t)_{\partial\Omega_{FEM_T}} = E(x,t)_{\partial\Omega_{\omega_{0T}}}. \tag{7.14}$$

We choose the time step $\tau = 0.02$ in all tests correspondingly to the CFL condition (6.2). The penalty factor s is always choosen to be 1. In the initialized plane wave (7.9) we take $\omega = 7$ in all tests.

First, in the Test 3 we demonstrate that our computed solution E_h in the domain decomposition method approximates very good the exact solution E in the case when $\varepsilon = \mu = 1$ in Ω. Next, in the Test 4 we demonstrate the validity of our method on simulation of the problem (7.10), (7.11)- (7.14) in the presence of the function $\varepsilon(x) \neq 0$ in Ω_{FEM}.

7.2.1. Test 3. In this test we compare our computational solution obtained in the domain decomposition method with the analytical solution. We compute the problem (7.10), (7.11)-(7.14) on two different meshes with different mesh sizes h, with $h = 0.125$ and with $h = 0.05$. The plane wave is defined as in (7.9).

The analytical solution of the problem (7.10), (7.11)-(7.14) with $\varepsilon = \mu = 1$ reduces to the solution of the homogeneous wave equation and is given by the following formula, see [8]:

$$E_2(y,t) = \begin{cases} 0, & \text{if } t \in (0, a-y). \\ \sin\omega\,(t-a+y), & \text{if } t \in \big(a-y, a-y+\frac{2\pi}{\omega}\big), \\ 0, & \text{if } t > a-y+\frac{2\pi}{\omega}. \end{cases} \tag{7.15}$$

where y is the vertical coordinate and we consider the problem (7.10), (7.11)- (7.14) in the domain $R_a = \{y < a\}, a = const. \geq 0$, while $E_1 = 0$.

Figure 7.13 presents comparison between the exact solution given by (7.15) and the computed solutions for the problem (7.10), (7.11)-(7.14), at different points of the computational domain Ω. We show the

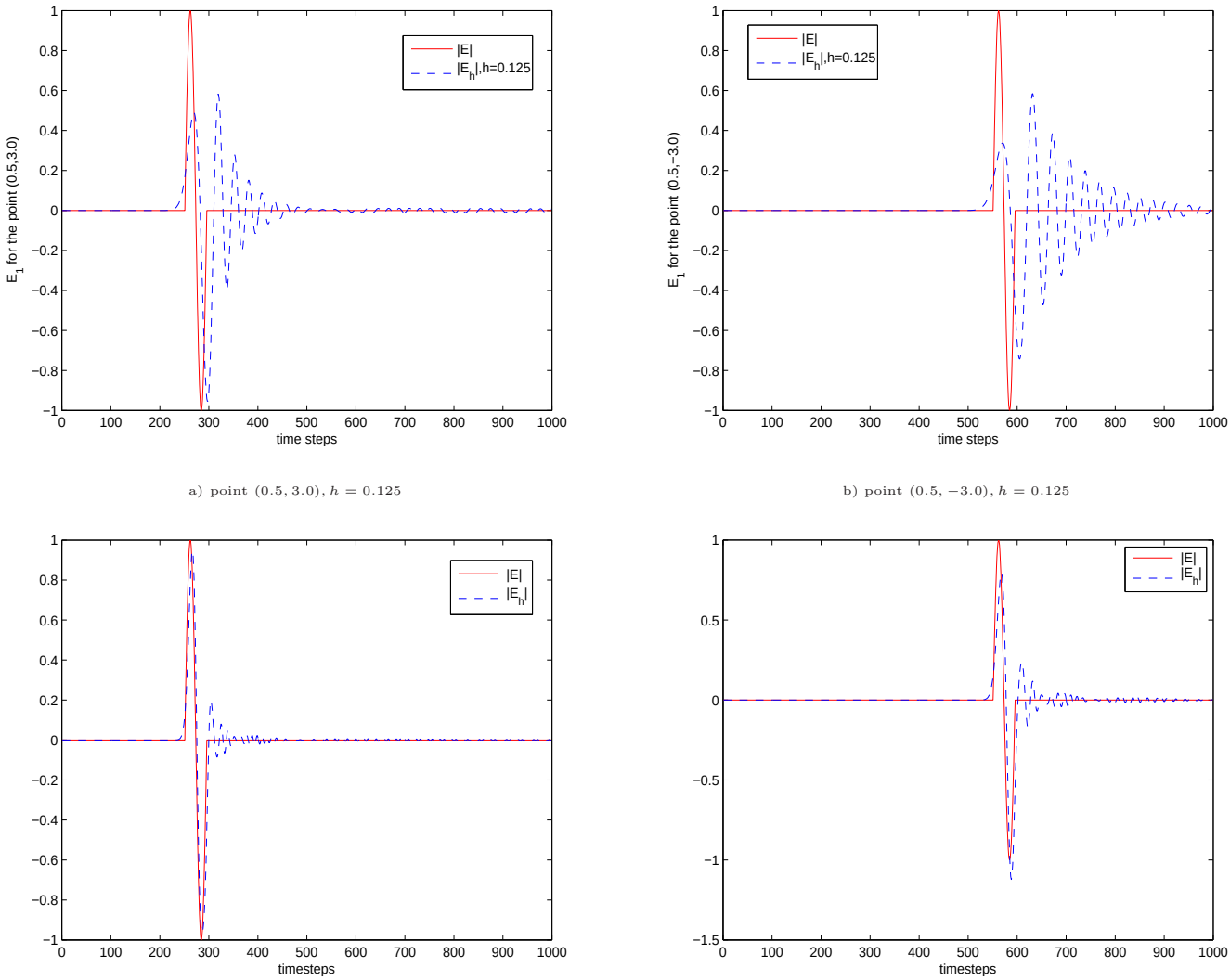

a) point $(0.5, 3.0)$, $h = 0.125$

b) point $(0.5, -3.0)$, $h = 0.125$

c) point $(0.5, 3.0)$, $h = 0.05$

d) point $(0.5, -3.0)$, $h = 0.05$

Fig. 7.13: *Test 3. Comparison of the analytic and the computed solution in the domain decomposition FEM/FDM method in time* $T = (0, 20)$ *with* $\varepsilon = \mu = 1$. *We show computed domain decomposition solution on different meshes with mesh sizes* h *: a) on the mesh with* $h = 0.125$ *at the point* $(0.5, 3.0)$, *which is located at the upper part of the computational domain* Ω_{FEM}*; b) on the mesh with* $h = 0.125$ *at the point* $(0.5, -3.0)$, *which is located at the lower of the* Ω_{FEM}*; c) for the mesh size* $h = 0.05$ *at the point* $(0.5, 3.0)$*; c) for the mesh size* $h = 0.05$ *at the point* $(0.5, -3.0)$*;*

computed domain decomposition solution on different meshes with mesh sizes $h = 0.125$ and $h = 0.05$. We observe that the exact and the computed solutions have main difference at the bottom of the computational domain Ω_{FEM}. This can be explained by the fact that the computational error grows with the computational time. Comparing 7.13-a),b) with 7.13-c),d) we observe that the computed solution E_h on the mesh with the mesh size $h = 0.125$ has approximately twice smaller amplitude than the exact solution E, but the computed solution on the mesh size $h = 0.05$ approximates more accurately the exact solution. The same observation confirms the Figure (7.12)-a) which shows the comparison of the exact norm $||E||_{\Omega_{FEM}}$ and the computed

norm $||E_h||_{\Omega_{FEM}}$ on different meshes with mesh sizes $h = 0.125$ and $h = 0.05$ in the time $T = (0, 20)$.

This test shows that the used FEM scheme in the domain decomposition method is the second order convergent in space and time, and the underlaying a posteriori error analysis for (7.11)-(7.14) is similar to the one developed in [3].

7.2.2. Test 4. The goal of this test is to explain why in some real-life experiments with the electromagnetic plane wave which propagates in the medium with the coefficient $\varepsilon \neq 0$ it is still possible approximate the Maxwell's system with the wave equation

$$\begin{aligned} \varepsilon \frac{\partial^2 E}{\partial t^2} + \triangle E = 0, \text{ in } \Omega_T, \\ E(x,0) = f_0(x), \quad E_t(x,0) = 0 \text{ in } \Omega, \\ E(x,t) = f(t), \text{ on } \partial\Omega_1 \times (0,t_1], \\ \partial_n E(x,t) = -\partial_t u(x,t), \text{ on } \partial\Omega_1 \times (t_1,T), \\ \partial_n E(x,t) = -\partial_t u(x,t), \text{ on } \partial\Omega_2 \times (0,T), \\ \partial_n u(x,t) = 0, \text{ on } \partial G_3 \times (0,T). \end{aligned} \tag{7.16}$$

Such model is considered in our recent publications [6, 16] where the spatially distributed dielectric constant was reconstructed from experimental data via a hybrid globally convergent/adaptive algorithm. In [6, 16] was pointed out that some discrepancies in the computational model and the reality was used: instead of the considering of the globally convergent method for the Maxwell's system (3.2)- (3.5) was used the model of the single wave equation (7.16). Moreover, it was not known which one of the components of the electric field was measured in experiments. The fact that in [6, 16] still was obtained very accurate reconstruction of the dielectric constant demonstrates validity of the approximated model. Our test below demonstrates explanation of the experiment in [6, 16].

We initialize a plane wave f as in (7.9) which is similar to the time-resolved electromagnetic signal used in experiments of [6, 16]. Next, we solve the problem (7.10), (7.11)- (7.14) with the coefficient ε in Ω_{FEM} defined as

$$\varepsilon = \begin{cases} 1 + 0.5(\sin(\frac{\pi}{3}x))^2 \cdot (\sin(\pi/3)y)^2, & -3 \le x < 0, \quad \text{and} \quad -3 \le y < 3; \\ 1 + 0.5(\sin(\frac{\pi}{3}x))^2 \cdot (\sin(\pi/3)y)^2, & 0 \le x \le 3, \quad \text{and} \quad 0 \le y \le 3; \\ 1 + A(\sin(\frac{\pi}{3}x))^2 \cdot (\sin(\pi/3)y)^2, & 0 \le x \le 3, \quad \text{and} \quad -3 \le y \le 0; \end{cases} \tag{7.17}$$

where $A = 4.0, 12.0, 26.0$, see Figure 7.11.

Figures 7.16-7.17 show how the plane wave propagates in Ω with ε in Ω_{FEM} given by (7.17) with $A = 4.0$, see Fig. 7.11-a). We observe that the plane wave f is initialized at the top boundary $\partial\Omega_1$ and propagates into Ω for $t \in (0, t_1]$. First order absorbing boundary conditions [10] are used on the top $\partial\Omega_1 \times (t_1, T]$ and the bottom $\partial\Omega_2 \times (0, T]$ boundaries, and Neumann or mirror boundary condition is used on $\partial\Omega_3 \times (0, T]$. Figures 7.16-7.17 demonstrate also the continuity of the numerical solution in the domain decomposition method across the FD/FE mesh. We observe that the electric field $E = (E_1, E_2)$ as also the intensity of the electric field $|E_h| = \sqrt{E_{1h}^2 + E_{2h}^2}$ remains smooth across the FE/FD interface.

Using the Figures 7.16-7.16 we can conclude that the maximum of the component E_2, where the plane wave was initialized, is about three times higher than the maximum of the component E_1 at all times. Figure (7.12)-b) shows comparison of the computed norms $||E_{1h}||$ and $||E_{2h}||$ in the time $T = (0, 20)$ in Ω_{FEM}. In these computations we have used amplitudes $A = 4, 12, 26$ in the definition (7.17) of the coefficient ε inside Ω_{FEM}. From the Figure (7.12)-b) we can conclude that the computed solution E_h does not contain spurious solutions as soon as values of the coefficient ε are not too big (the amplitude $A < 12$ in (7.17)), and the final time T is also not very large ($T < 12$).

Thus, all meaningful reflections from the coefficient ε are from the component E_2 while the reflections from the another component E_1 are negligible compared with the reflections from the component E_2. This fact explains why in experiments of [6, 16] was possible to measure only the single time-resolved signal and

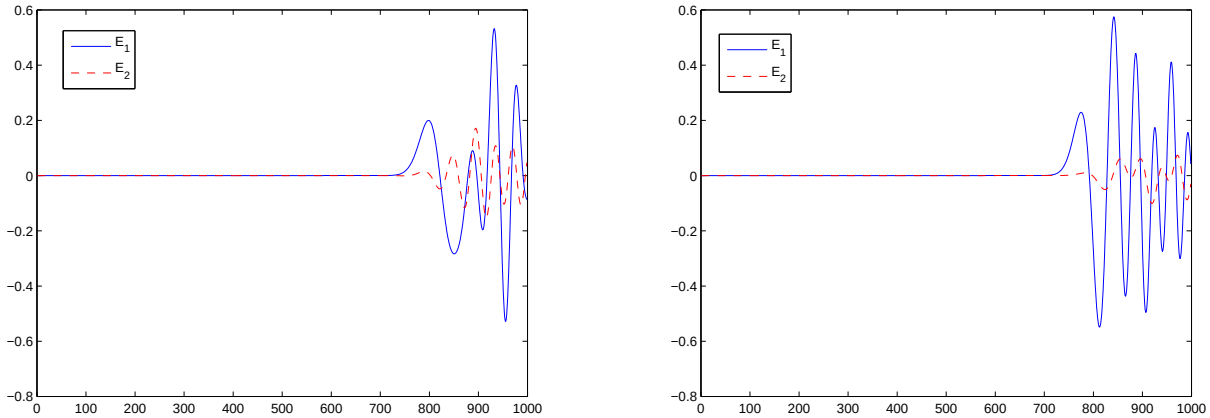

a) b)

Fig. 7.14: *Test 4: Behaviour of the computed solution* $E_h = (E_{1h}, E_{2h})$ *in time* $T = (0, 20)$ *for the equation (7.11)-(7.14) on the mesh with the mesh size* $h = 0.125$ *at different points at the FEM/FDM boundary : a) at the point* $(1.0, -3.5)$*; b) at the point* $(1.5, -3.5)$*. Here the horizontal axis denotes the the number of time steps in time* $T = (0, 20)$ *and* $E_1 = E_2, E_2 = E_1$*.*

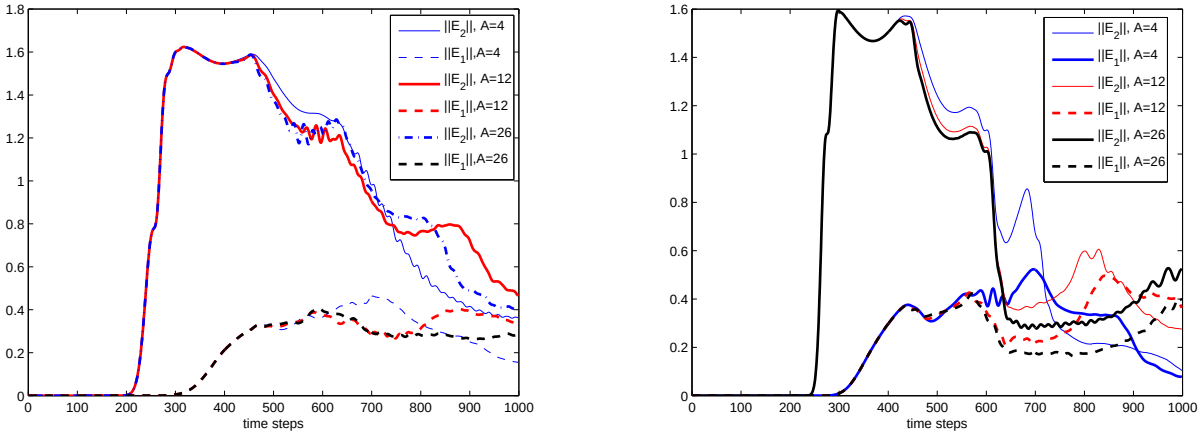

a) $h = 0.125$ b) $h = 0.05$

Fig. 7.15: *Test 4: comparison of the computed* L_2*-norms for* $||E_{1h}||$ *and for* $||E_{2h}||$ *on different meshes with mesh sizes* $h = 0.05$ *and* $h = 0.125$ *in time* $T = (0, 20)$ *in* Ω_{FEM}*. Computations are performed with different amplitudes* A *in the definition (7.17) of the coefficient* ε *inside* Ω_{FEM}*. Here the horizontal axis denotes the the number of time steps in time* $T = (0, 20)$*.*

why the another two components of the 3D test could not be measured - these remaining components was negligible compared to the first one component.

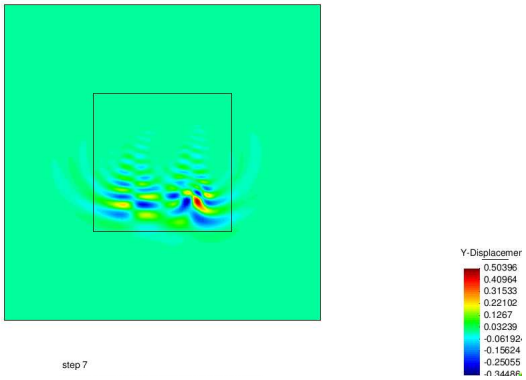

a) $T = 14$, E_1

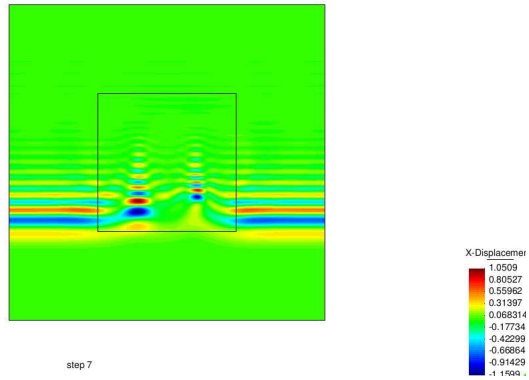

b) $T = 14$, E_2

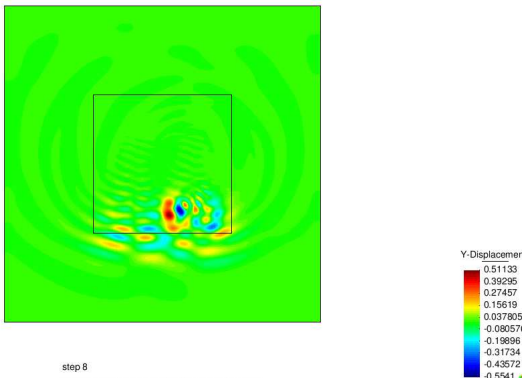

a) $T = 16.0$, E_1, $t = 16.0$

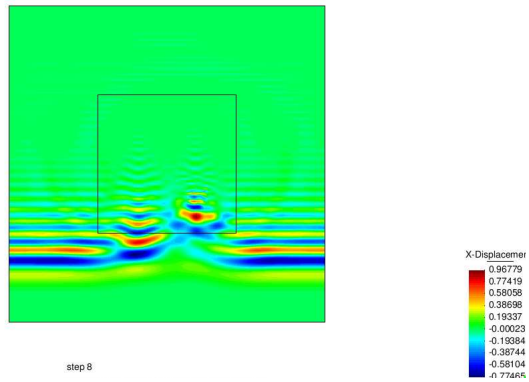

b) $T = 16.0$, E_2

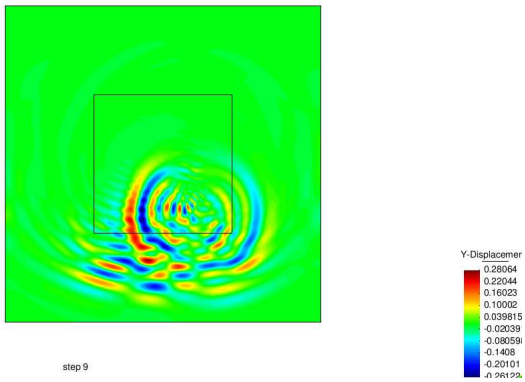

a) $T = 18.0$, E_1

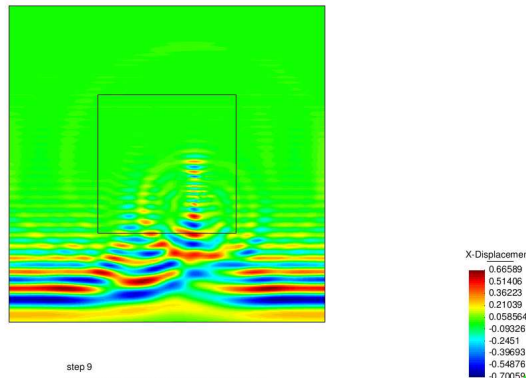

b) $T = 18.0$, E_2

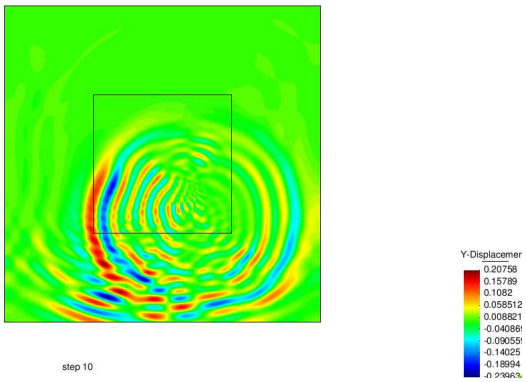

a) $T = 20.0$, E_1

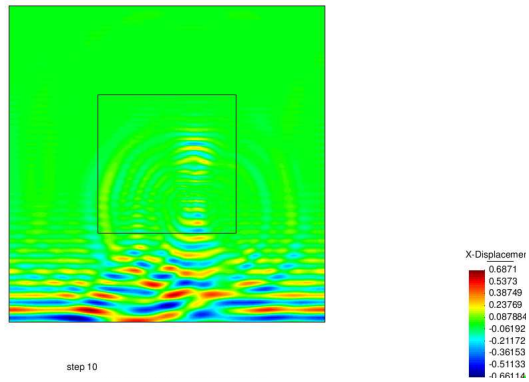

b) $T = 20.0$, E_2

Fig. 7.16: *Test 4: Computed components of the electric field* $E_h = (E_{1h}, E_{2h})$ *with* $h = 0.125$ *at different times in* Ω *using the domain decomposition FEM/FDM method. The coefficient* ε *in* Ω_{FEM} *is defined by (7.17).*

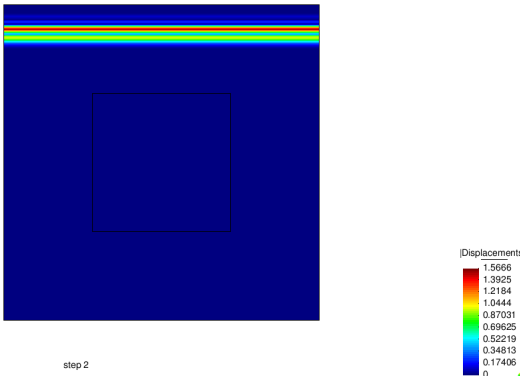

a) $t = 4.0$

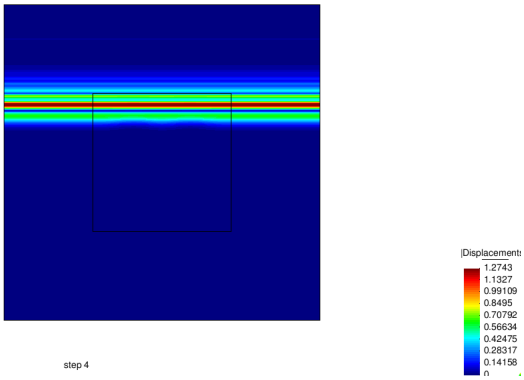

b) $t = 8.0$

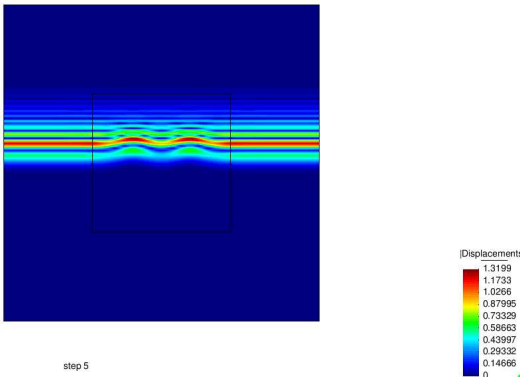

a) $t = 10.0$

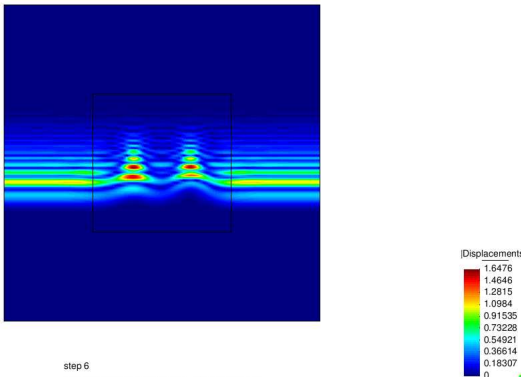

b) $t = 12.0$

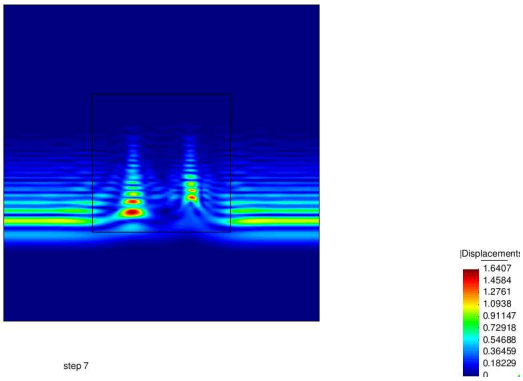

a) $t = 14.0$

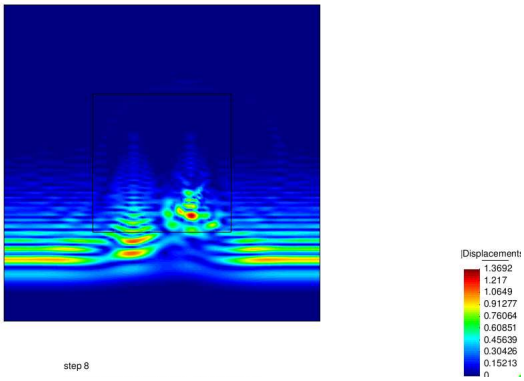

b) $t = 16.0$

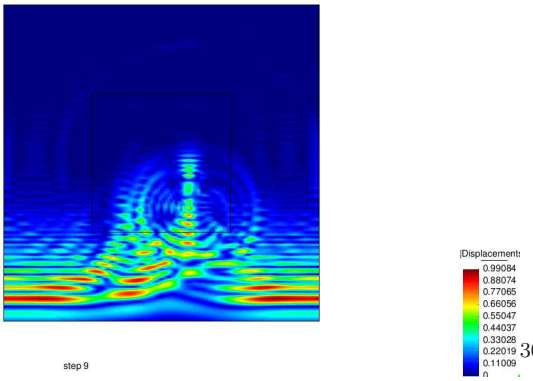

a) $t = 18.0$

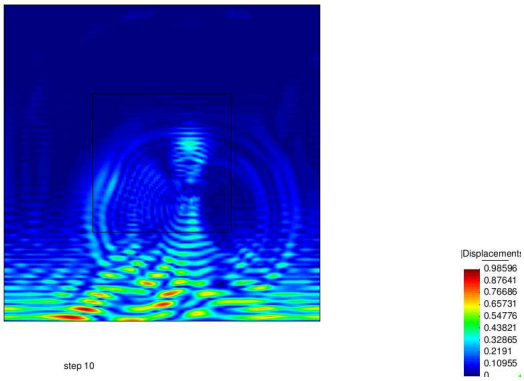

b) $t = 20.0$

Fig. 7.17: *Test 4: Intensity of the electric field* $|E_h| = \sqrt{E_{1h}^2 + E_{2h}^2}$ *on the mesh with the mesh size* $h = 0.125$ *at different times in* Ω*. The coefficient* ε *in* Ω_{FEM} *is defined by (7.17).*

Acknowledgments

This work was supported by the Swedish Foundation for Strategic Research (SSF) at Gothenburg Mathematical Modeling Center (GMMC) and by the Swedish Institute, Visby program. The author acknowledges also Mohammad Asadzadeh for useful discussions and suggestions.

REFERENCES

[1] F. Assous, P. Degond, E. Heintze and P. Raviart, (1993), On a finite-element method for solving the three-dimensional Maxwell equations, J.Comput.Physics, 109, pp.222–237.

[2] L. Beilina, K. Samuelsson, K. Åhlander, Efficiency of a hybrid method for the wave equation. *Proceedings of the International Conference on Finite Element Methods: Three dimensional problems*. GAKUTO international Series, Mathematical Sciences and Applications, V. 15, 2001.

[3] L. Beilina, M. Grote, Adaptive Hybrid Finite Element/Difference Method for Maxwell's equations, *TWMS J. of Pure and Applied Mathematics*, V.1(2), pp.176-197, 2010.

[4] L. Beilina, C. Johnson C 2001 A hybrid FEM/FDM method for an inverse scattering problem. In *Numerical Mathematics and Advanced Applications - ENUMATH 2001*. Springer-Verlag.

[5] L. Beilina, C. Johnson, A posteriori error estimation in computational inverse scattering, *Mathematical Models and Methods in Applied Sciences*, 15, 23-37, 2005.

[6] L.Beilina, M.V.Klibanov, Reconstruction of dielectrics from experimental data via a hybrid globally convergent/adaptive inverse algorithm, *Inverse Problems*, 26, 125009, 2010.

[7] S. C. Brenner, L. R. Scott, (1994), The Mathematical theory of finite element methods, Springer-Verlag.

[8] Budak B M, Samarskii A A and Tikhonov A N 1988 *A Collection of Problems in Mathematical Physics* (New York: Dover Publications)

[9] A. Elmkies and P. Joly, (1997), Finite elements and mass lumping for Maxwell's equations: the 2D case, Numerical Analysis, C. R. Acad.Sci.Paris, 324, pp. 1287–1293.

[10] Engquist B and Majda A, (1977), Absorbing boundary conditions for the numerical simulation of waves *Math. Comp.* **31**, pp.629-651

[11] T. J. R. Hughes, (1987), The finite element method, Prentice Hall.

[12] B. Jiang, (1998), The Least-Squares Finite Element Method, Theory and Applications in Computational Fluid Dynamics and Electromagnetics, Springer-Verlag, Heidelberg.

[13] B. Jiang, J. Wu and L. A. Povinelli, (1996), The origin of spurious solutions in computational electromagnetics, J. Comput. Phys., 125, pp.104–123.

[14] J. Jin, (1993), The finite element method in electromagnetics, Wiley.

[15] P. Joly, (2003), Variational methods for time-dependent wave propagation problems, Lecture Notes in Computational Science and Engineering, Springer.

[16] M.V. Klibanov, M.A. Fiddy, L. Beilina, N. Pantong and J. Schenk, Picosecond scale experimental verification of a globally convergent numerical method for a coefficient inverse problem, *Inverse problems*, 26, 045003, 2010.

[17] O.A. Ladyzhenskaya, *Boundary Value Problems of Mathematical Physics*, Springer, Berlin, 1985.

[18] P. B. Monk, (2003), Finite Element methods for Maxwell's equations, Oxford University Press.

[19] P. B. Monk and A. K. Parrott, (1994), A dispersion analysis of finite element methods for Maxwell's equations, SIAM J.Sci.Comput., 15, pp.916–937.

[20] P. B. Monk, (1992), A comparison of three mixed methods, J.Sci.Statist.Comput., 13.

[21] C. D. Munz, P. Omnes, R. Schneider, E. Sonnendrucker and U. Voss, (2000), Divergence correction techniques for Maxwell Solvers based on a hyperbolic model, J.of Comp.Phys., 161, pp.484–511.

[22] K. D. Paulsen, D. R. Lynch, (1991), Elimination of vector parasites in Finite Element Maxwell solutions, IEEE Trans.Microwave Theory Tech.,39, 395 –404.

[23] I. Perugia, D. Schötzau, The hp-local discontinuous Galerkin method for low-frequency time-harmonic Maxwell equations, *Mathematics of Computation*, V.72, N.243, pp.1179-1214, 2002.